


Open thermal convection dolomitization: an example from East Yunnan (China)

Jing-Qi Zhang , Zhen-Kui Jin, Xiao-Er Zhu, Yang Li, Qi-Heng Guo and Shu-Ting Shi

College of Geosciences, China University of Petroleum, Beijing 102249, China

Original Article

Cite this article: Zhang J-Q, Jin Z-K, Zhu X-E, Li Y, Guo Q-H, and Shi S-T (2021) Open thermal convection dolomitization: an example from East Yunnan (China). *Geological Magazine* **158**: 330–348. <https://doi.org/10.1017/S0016756820000503>

Received: 26 December 2018

Revised: 23 April 2020

Accepted: 27 April 2020

First published online: 5 June 2020

Keywords:

dolostone; dolomitization; thermal convection; Emei mantle plume; middle Permian; East Yunnan

Author for correspondence:

Zhen-kui Jin, Email: jinzhenkui@188.com

Abstract

Dolostones are widely developed in the middle Permian rocks of East Yunnan, China, mainly in the shoal-facies Maokou Formation. The previously reported dolostone formation mechanisms cannot explain the distribution and geochemical characteristics of these dolostones, in particular their strontium, magnesium and oxygen isotope signatures. To help predict the distribution of dolostone reservoirs and reduce the exploration risk and cost, this study proposes a new model of dolomitization: open thermal convection dolomitization. In this new dolomitization model, Mg^{2+} in dolomitizing fluids originates mostly from seawater, with a minor component coming from deep hydrothermal fluids. Elevated heat flux (in this case due to the nearby Emei mantle plume) causes spatial temperature variations in the fluid along the circulation flow pathways, resulting in fast and pervasive dolomitization of limestone. The proposed model not only explains the characteristics and distribution of dolostones in the study area but also serves as a reference for predicting the distribution of dolostones in other areas subjected to thermal convection.

1. Introduction

Dolostones often form high-quality hydrocarbon reservoirs, containing more than half the hydrocarbons in carbonate rocks worldwide. In North America, up to 80% of carbonate-hosted hydrocarbons are hosted in dolostones (Zenger & Dunham, 1980; Sun, 1995). In China, carbonate-hosted hydrocarbons are concentrated almost entirely in dolostones (Zheng *et al.* 2007, 2008; Huang *et al.* 2012b). Studying the genesis of dolostones can therefore help predict the distribution of dolostone reservoirs and reduce the risk and cost of hydrocarbon exploration.

As early as 1779, the Italian scholar Arduinon investigated the genesis of dolostones in the Tyrolean Alps in southern Italy. He reported that the dolostones were generated from the *in situ* reaction between limestone and magnesium-rich hydrothermal fluid (Morlot, 1847). In the middle of and in the late twentieth century, many research studies on dolostone were conducted worldwide and several dolostone formation mechanisms were proposed. These included the seepage reflux model (Adams & Rhodes, 1960; Deffeyes *et al.* 1965, p. 71–88), sabkha model (Friedman & Sanders, 1967; Hsu & Siegenthaler, 1969), burial model (Illing, 1959; Kohout *et al.* 1977, p. 1–34; Oliver, 1986; Tóth, 1988; Wilson *et al.* 1990; Garven, 2003), mixing zone model (Land, 1972; Badiozamani, 1973), hydrothermal dolomitization (Anderson & Garven, 1987; Cervato, 1990; Mountjoy & Halim-Dihardja, 1991; Davies & Smith, 2011), and microbial/organogenic model (Vasconcelos & McKenzie, 1997; Burns *et al.* 2000; Mazzullo, 2000; Kenward *et al.* 2012). Other scholars have comprehensively reviewed the genesis of dolostones (Zenger & Hardie, 1987; Machel, 2004; Zhang *et al.* 2006; Wang *et al.* 2013).

In the early 1990s, as the hydrocarbon exploration focus in China shifted from continental facies to marine facies, dolostones gradually received more attention from Chinese scholars. Among these dolostones, the middle Permian dolostones in the western region of the Yangtze platform are among the most important rock units for hydrocarbon exploration in Chinese marine carbonates. A series of studies were conducted on the genesis of these dolostones, and various dolostone formation mechanisms have been proposed including the mixing zone model (Zhang, 1982; Song, 1985; Chen, 1989), burial model (He & Feng, 1996; Wang & Jin, 1997; Jiang *et al.* 2014), basalt leaching dolomitization model (Jin & Feng, 1999), structurally controlled hydrothermal dolomitization model (Huang *et al.* 2012a) and hydrothermal dolomitization model (Wang *et al.* 2014). However, these previously proposed dolostone formation mechanisms cannot reasonably explain the distribution and geochemical characteristics of the middle Permian dolostones in the western region of the Yangtze platform.

We therefore propose a new dolomitization model: open thermal convection dolomitization. Unlike existing thermal convection models, the dolomitization model proposed here is related to the mantle plume and the scale of dolomitization is very large. In addition, the distribution of dolostones in this thermal convection model is controlled by sedimentary facies and the dolomitization is selective. The proposed model not only explains the characteristics and distribution

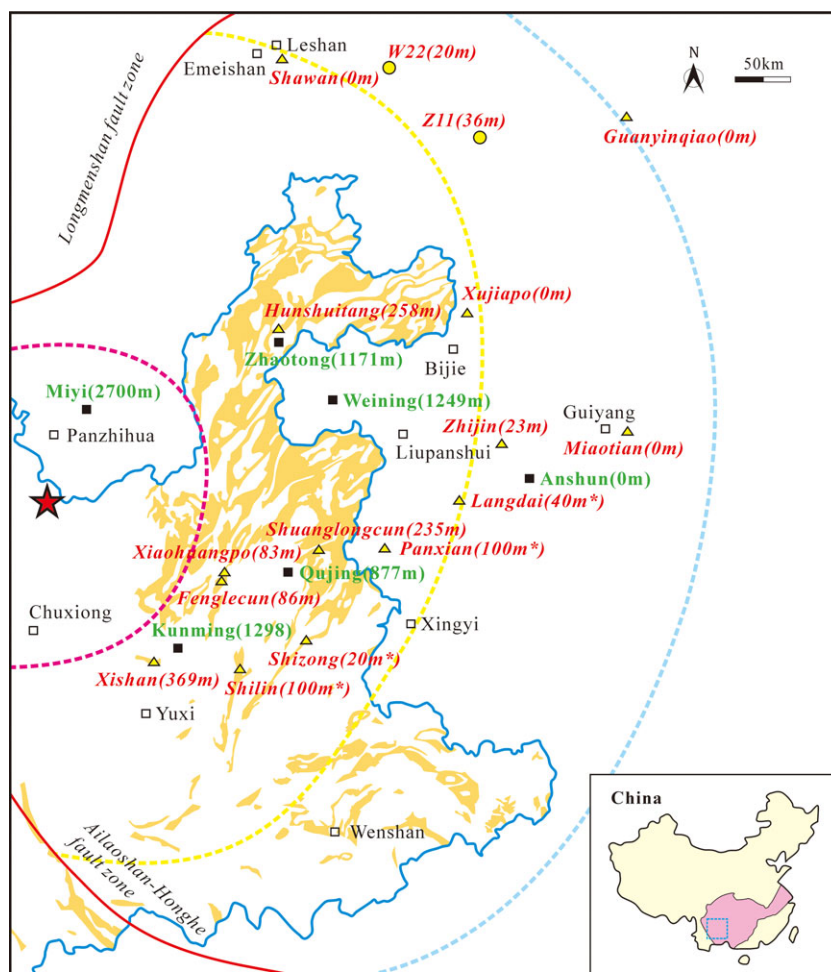


Fig. 1. (Colour online) Geological map of East Yunnan overlain by the upper Permian Emei basalt and middle Permian dolostones. Asterisk: data estimated by combining various types of data (as a result of complex geological conditions, including challenging access, it was difficult to precisely measure the thicknesses of dolomitized rocks (e.g. massive dolostone, patchy dolostone and patchy limestone)).

of dolostones in the study area, but also serves as a reference to predict the distribution of dolostones in other areas subjected to thermal convection.

2. Geological setting

East Yunnan constitutes the western region of the Yangtze platform. With an area of 1.8×10^5 km², East Yunnan is located in Yunnan Province on the southeastern side of the Longmenshan fault zone and the northeastern side of the Ailaoshan–Honghe fault zone (Ministry of Geology and Mineral Resources of PR China, 1982, p. 1–3) (Fig. 1). East Yunnan’s Permian strata are mainly exposed in its northeastern part (Fig. 1).

The Permian trisection scheme was used here as a stratigraphic scheme (Li *et al.* 2005). Lower Permian strata are generally absent in East Yunnan. The middle Permian strata can be divided into the Liangshan Formation (oldest), Qixia Formation and Maokou Formation (youngest). The Liangshan Formation unconformably overlies Carboniferous strata, and conformably contacts the overlying Qixia Formation. The Maokou Formation conformably contacts the underlying Qixia Formation and unconformably contacts the overlying upper Permian strata (Fig. 2). Note that the

middle Permian strata of the Yangtze platform corresponds to the Guadalupian and Kungurian of the international stratigraphic standard (Fig. 2) (Li *et al.* 2005), which corresponds to the period 284–259 Ma (<http://www.stratigraphy.org/index.php/ics-chart-timescale>).

The Liangshan Formation is 2–20 m thick and contains marine and terrigenous facies, including carbonaceous shale mixed with mudstone, siltstone and limestone lenses (Ministry of Geology and Mineral Resources of PR China, 1982, p. 164; Jin & Feng, 1999).

The Qixia Formation is 50–200 m thick and comprises medium- to thin-bedded carbonates: dark-grey to grey bioclastic packstone, bioclastic wackestone and dolostone. The palaeowater depth is interpreted to have been relatively deep (Ministry of Geology and Mineral Resources of PR China, 1982, p. 164–165; Jin & Feng, 1999).

The Maokou Formation is 100–500 m thick and is dominated by thick-bedded to massive, grey to light-grey bioclastic grainstone, dolostone and bioclastic packstone. The palaeowater depth is interpreted to have been relatively shallow (Ministry of Geology and Mineral Resources of PR China, 1982, p. 165; Jin & Feng, 1999). The Maokou Formation, which hosts most of the middle Permian dolostone in East Yunnan, has experienced substantial dolomitization during its geological history.

System	Series		Stage	Formation			
	Global	Local					
Permian	Lopingian	Upper	Changxing Stage	Xuanwei Formation	Changxing Formation	Dalong Formation	
			Wujiaping Stage	Emei Basalt	Longtan Formation	Wujiaping Formation	
	Guadalupian	Middle	Maokou Stage	Maokou Formation			
			Qixia Stage	Qixia Formation			
	Cisuralian	Lower	Longlin Stage	Liangshan Formation			
			Zisong Stage	Lacuna			

Fig. 2. Permian stratigraphic subdivisions in East Yunnan. The unconformities are represented by dotted lines.

During the early middle Permian period, East Yunnan and the entire Upper Yangtze platform began to settle and transgression occurred. This transgression initiated the deposition of the Liangshan Formation, which extended over existing Carboniferous, Devonian and older strata. During the development of the Qixia and Maokou formations, the main environments of East Yunnan existed in those rocks as open-platform facies (Jin & Feng, 1999; Chen *et al.* 2011).

During the late middle Permian period, the Dongwu movement, which is the rapid differential crustal uplift caused by the rising of the Emei mantle plume, affected southern China (He *et al.* 2005b). As a result of the activity of the Emei mantle plume, the whole Yangtze platform was uplifted, resulting in a regional unconformity between middle Permian and upper Permian rocks (He *et al.* 2005b). Simultaneously, a large-scale basic magmatic eruption occurred in the western Yangtze platform, forming thick Emei basalt (64–5386 m thick) (Ministry of Geology and Mineral Resources of PR China, 1982, p. 165). According to previous research results, the active area of the Emei mantle plume can be divided into an inner belt, a middle belt and an outer belt from west to east (He *et al.* 2003, 2005a; Luo *et al.* 2012). From the inner belt to the outer belt, the activity intensity of the Emei mantle plume gradually weakened. This weakening produced a corresponding and gradual reduction in the thicknesses of denudation of the Maokou Formation and the erupted Emei basalt (Fig. 1). During this stage, East Yunnan was dominated by extensional movement; basement faults were reactivated and tensional faults, strike-slip faults and fracture systems developed (Luo *et al.* 1988; Liu & Zhu, 2009).

In the early late Permian period, transgression occurred again in East Yunnan, and upper Permian rock deposition commenced.

The crustal uplift and basaltic eruption caused by Emei mantle plume activity significantly altered the depositional pattern of East Yunnan. From west to east, fluvial–alluvial plain facies, tidal flat–lagoon facies and carbonate platform facies were developed (Fig. 3) (Jin & Feng, 1999; Chen *et al.* 2011).

Notably, the geological conditions in the study area are complex, with Permian strata being poorly exposed because of local limestone mining and small dip angles of the strata, mostly between 3 and 30° (Ministry of Geology and Mineral Resources of PR China, 1982, p. 175). In addition, the perennial rain of the region has caused significant erosion and weathering of the strata, adding difficulties to this research. By combining various petrological and geochemical methods, we attempt to make the best use of existing data to analyse the formation mechanism of these middle Permian dolostones and propose a reasonable and reliable dolomitization model.

3. Methods

The middle Permian samples studied here were collected from the Hunshuitang, Shuanglongcun, Xiaohuangpo, Fenglecun, Xishan, Shizong, Shilin, Shawan, Guanyinqiao, Xujiapo, Zhijin, Miaotian, Langdai and Panxian sections. Well Z11 and Well W22 also provided samples. The first seven sections are located in East Yunnan; the remaining seven sections and the wells are situated in Sichuan and Guizhou provinces, which are geographically close to East Yunnan. A total of 217 outcrop samples and 12 well samples were studied.

The strata thickness data of outcrop sections were obtained in two ways: (1) actual measurement by using measuring tape, geological compass, global positioning system (GPS) receiver and geological map for 10 outcrops (without an asterisk in Fig. 1); (2) estimated by combining GPS data, strata attitude data, geological map and photograph for four outcrops (with an asterisk in Fig. 1). The strata thickness data of well profiles were provided by Sinopec Group and China National Petroleum Corporation.

Petrographic studies on the 610 uncovered thin-sections (thickness, 30 µm) were performed using polarizing microscopy. A total of 562 thin-sections were stained with Alizarin red S (0.1 g Alizarin red S per 100 mL 0.2% hydrochloric acid) and 48 thin-sections were stained with Alizarin red S and potassium ferricyanide (0.12 g Alizarin red S and 0.8 g potassium ferricyanide per 100 mL 1.5% hydrochloric acid).

Cathodoluminescence (CL) observations were performed on 93 polished thin-sections at the State Key Laboratory of Geological Processes and Mineral Resources of the China University of Geosciences (Beijing) using a CITL CL8200 MK5 optical CL System (Cambridge Image Technology Limited, Welwyn Garden City, UK) operating at 12 kV and 300 µA, with an exposure time of 2 s. All samples were subjected to the same test conditions to facilitate the comparison of results.

Order degree values of the dolostones were measured for 30 powdered samples at the State Key Laboratory of Petroleum Resources and Prospecting of the China University of Petroleum (Beijing) using a Bruker AXS D2 Phaser (Bruker AXS GMBH, Karlsruhe, Germany). This procedure applied the computing method of Fuchtbauer (1974) to data collected using Cu K α radiation at a 2 θ of 4.5–50°, with a step size of 0.02° and scan time of 0.5 s for each step.

Fluid inclusion analysis was conducted on 10 thin-sections (33 inclusions) of 80 µm thickness at the Analytical Laboratory of the Beijing Research Institute of Uranium Geology using a Linkam THMSG600 heating–freezing stage (Linkam Scientific Instruments,

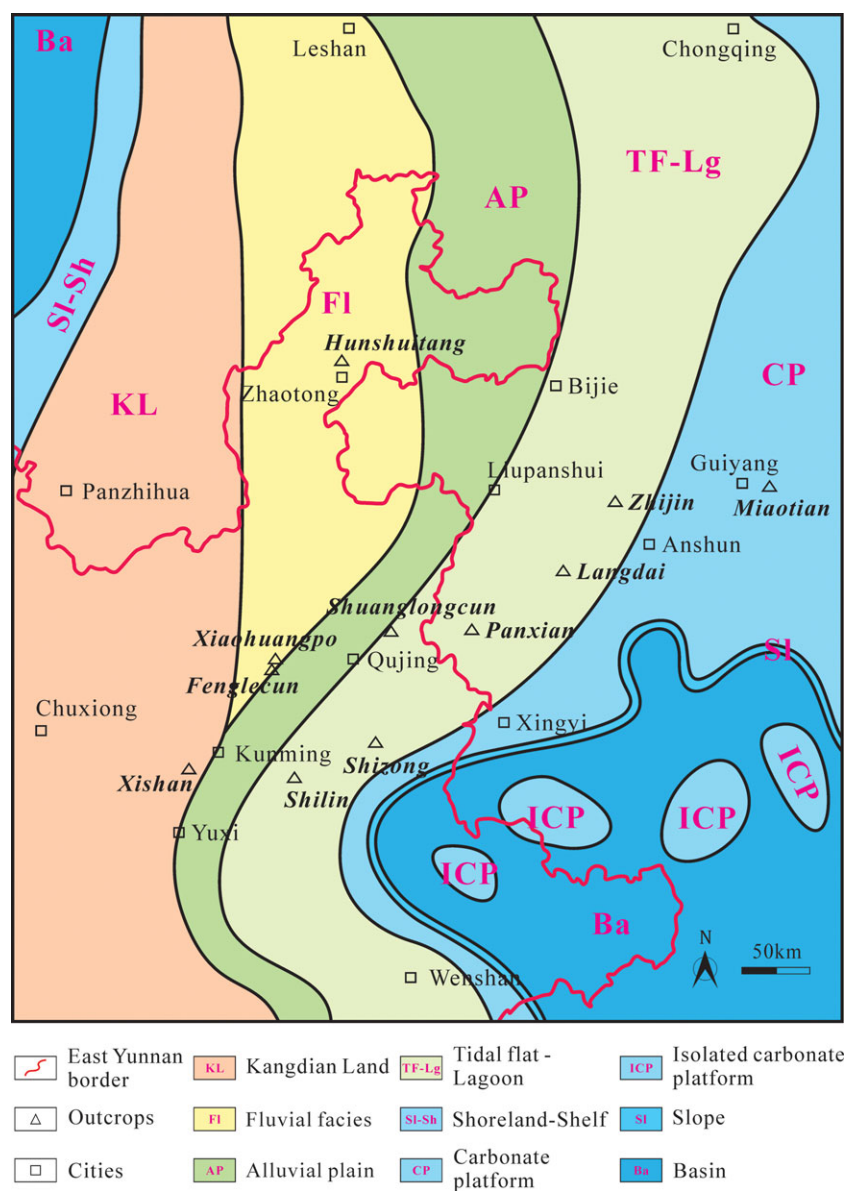


Fig. 3. (Colour online) Palaeogeography of the upper Permian strata in East Yunnan (modified from Feng *et al.* 1996; Chen *et al.* 2011).

Tadworth, UK) coupled with an Olympus polarizing microscope (Olympus Corporation, Tokyo, Japan), using the standard method described by Goldstein & Reynolds (1994). The temperature error was $\pm 1^\circ\text{C}$.

Carbon and oxygen isotopic compositions of the dolostones were measured for 25 powdered samples (particle size, $\leq 74\ \mu\text{m}$) at the Nanjing Institute of Geology and Palaeontology of the Chinese Academy of Sciences using a Finigan MAT 253 mass spectrometer with a Kiel IV Carbonate Device (Thermo Fisher Scientific, Waltham, Massachusetts, USA). Phosphoric acid of 100% purity was used in this study. The reaction temperature was $50.0 \pm 0.1^\circ\text{C}$ and the reaction time was 36 hours. Each sample was measured three times and the calibration standard was Chinese carbonate standard GBW-04405 ($\delta^{13}\text{C}_{\text{PDB}}$ value of $0.57 \pm 0.03\text{‰}$ and $\delta^{18}\text{O}_{\text{PDB}}$ value of $-8.49 \pm 0.14\text{‰}$). The standard deviations of $\delta^{13}\text{C}_{\text{PDB}}$ and $\delta^{18}\text{O}_{\text{PDB}}$ were 0.04‰ and 0.08‰ , respectively. The oxygen isotope composition of dolomite was calculated using the fractionation factor reported by Rosenbaum & Sheppard (1986). The isotopic ratios for carbon and oxygen were expressed

as $\delta^{13}\text{C}$ and $\delta^{18}\text{O}$ per mil (‰) relative to the Vienna Pee Dee Belemnite (VPDB) standard.

Strontium isotopic compositions of the dolostones were measured for 10 powdered samples (particle size, $\leq 74\ \mu\text{m}$) at the Analytical Laboratory of the Beijing Research Institute of Uranium Geology, using a Phoenix thermal ionization mass spectrometer (Isotopx Ltd, Cheshire, UK). The acid used in this study is HCl ($0.8\ \text{mol L}^{-1}$), and the dissolution time was 2 hours. Isolation and purification of strontium were performed via ion exchange chromatography using AG 50 W-X8H⁺ resin (Bio-Rad, Hercules, California, USA). The standardized $^{86}\text{Sr}/^{88}\text{Sr}$ ratio was 0.1194, and the calibration standard was NBS-987 ($^{87}\text{Sr}/^{86}\text{Sr}$ value of 0.71034 ± 0.00026). The experimental error on this spectrometer was $0.000011\text{--}0.000026$.

Magnesium isotopic compositions of the dolostones were measured for seven powdered samples at the Radioisotope Laboratory of the University of Queensland using a Nu Plasma HR multi-collector inductively coupled plasma mass spectrometer (MC-ICP-MS) (Nu Instruments, Wrexham, UK). This procedure employed a cooling gas flow rate of $16\ \text{L min}^{-1}$, an auxiliary gas flow rate of

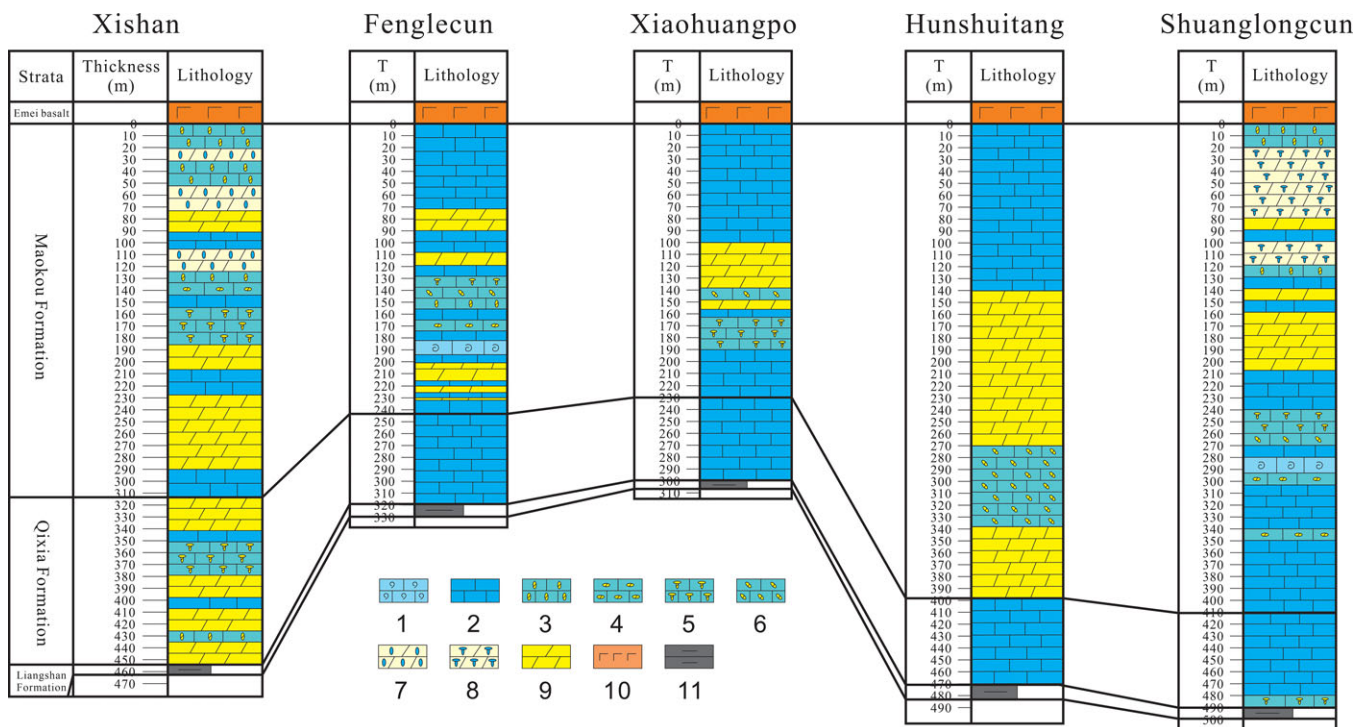


Fig. 4. (Colour online) Stratigraphic correlation of middle Permian sections in East Yunnan. The top surface of the middle Permian strata is flattened, and the section line is shown in Figure 5. 1, bioclastic grainstone; 2, bioclastic packstone; 3, patchy limestone with vertically elongated dolomite patches; 4, patchy limestone with parallel-elongated dolomite patches; 5, patchy limestone, containing grid-shaped dolomite patches; 6, patchy limestone, containing irregularly shaped dolomite patches; 7, patchy dolostone with vertically elongated dolomite patches; 8, patchy dolostone, containing grid-shaped dolomite patches; 9, dolostone (pure); 10, basalt; and 11, mudstone/shale.

0.8 L min^{-1} , a sample carrier gas flow rate of 1.1 L min^{-1} , an extraction voltage of -2000 V , a background ^{24}Mg value of 7 mV and a ^{24}Mg signal intensity of $32 \text{ V } (\mu\text{g/g})^{-1}$. Mg isotopic results are reported in standard δ -notation in per mil relative to DSM3 (Galy *et al.* 2003).

4. Results

4.a. Distribution characteristics of dolostones

Stratigraphically, the middle Permian dolostones of East Yunnan are mainly found in the Maokou Formation. In Xishan and Shuanglongcun outcrops, the Qixia Formation also contains some dolostones (Fig. 4). The dolomitized rocks of the Maokou and Qixia formations account for an average of 92.58% and 7.42% of the middle Permian dolomitized rocks, respectively. The average dolomitized proportions of the rocks of the Maokou and Qixia formations are 54.14% and 19.66%, respectively. The non-dolomitized strata comprise mainly dark-grey to grey bioclastic packstone (Fig. 4).

Note that the thickness of dolomitized rocks gradually decreases from the inner belt to the outer belt of the active area of the Emei mantle plume, and the dolomitization was not strictly controlled by faults (Fig. 5).

4.b. Petrographic characteristics of dolostones

The middle Permian dolostones in East Yunnan can be divided into two types based on their occurrence in single beds: massive dolostones (complete dolomitization, with dolomite content of 90–100%); and patchy dolostones (incomplete dolomitization, with dolomite content of 50–90%).

Massive dolostones are dark grey with no residual limestone in single bed, and some have slash marks. Vertically, the beds of

massive dolostone often alternate with the beds of limestone (mainly bioclastic packstone) (Figs 4, 6).

Patchy dolostones are grey or dark grey and contain dolomite and limestone patches (metasomatic remnants); dolomite patches constitute more than 50% of the rock volume, and the limestone patches are mainly bioclastic packstones. When the dolomite patch content falls below 50%, the patchy dolostones turn into patchy limestones (Fig. 7).

Dolomite patches vary in size from 0.5 cm to more than 1.5 m and exhibit various shapes (Fig. 7). Patchy dolostones/limestones can be divided into four types according to the patch shape: vertically elongated dolomite patches (i.e. dolomite patches perpendicular to the bedding planes); parallel-elongated dolomite patches (i.e. dolomite patches parallel to the bedding planes); grid-shaped dolomite patches; and irregularly shaped dolomite patches (Fig. 8).

Notably, the massive dolostones and patchy dolostones show similar microstructural characteristics (i.e. crystal size distribution, crystal size, crystal shape and CL) and geochemical characteristics (Table 1), with the only difference being the degree of dolomitization.

The crystal size distribution of the dolostones in the study area is mainly unimodal, and the crystals mainly comprise fine-grained (100–250 μm), medium-grained (250–500 μm) and coarse-grained (500–1000 μm) dolomite. The dolomite crystal shapes are mainly planar-subhedral and nonplanar-anhedral (Fig. 9a). Saddle dolomites with a ladder-like curved crystal face can be observed in a small number of samples (Fig. 9b).

In the study area, the ferroan dolomite is rare. In some samples, the dolomite preserves its original microstructural features from the limestone precursor (Fig. 9c, d). In some samples, scattered dolomites are relatively evenly distributed among calcites, but more enrichment is observed near stylolites (Fig. 9e), and the

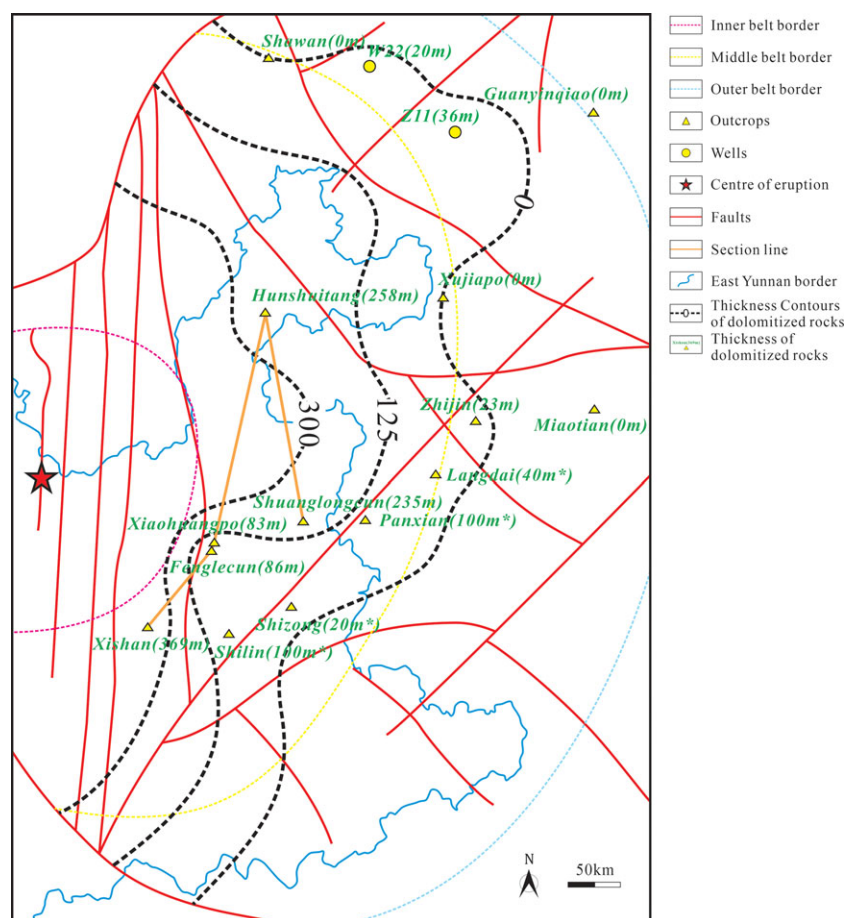


Fig. 5. (Colour online) Thickness map of the middle Permian dolomitized rocks in East Yunnan overlain by the upper Permian fault patterns (Luo *et al.* 1988, 2012). Asterisk: as in Figure 1.

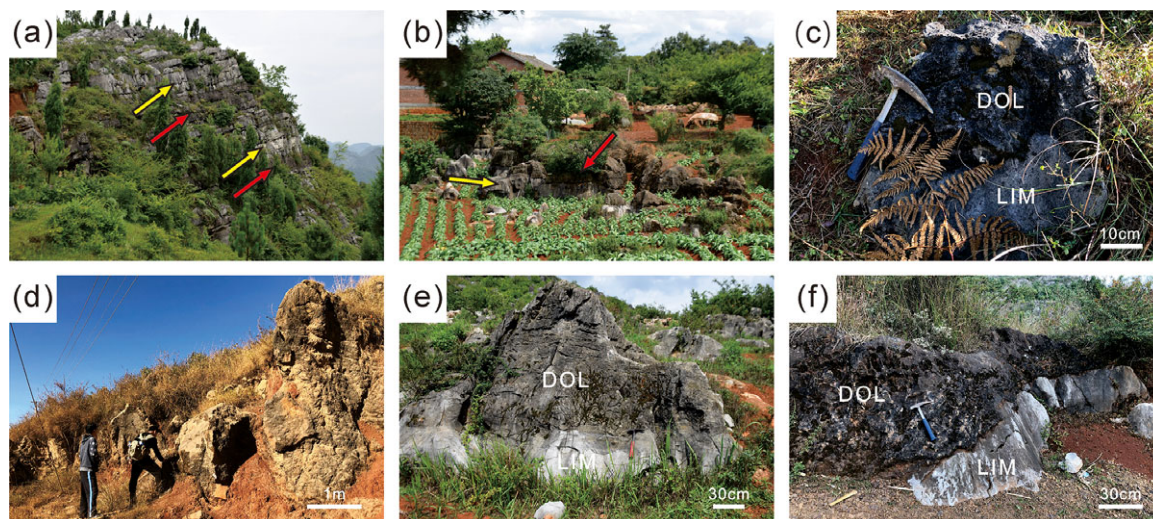


Fig. 6. (Colour online) Macroscopic characteristics of massive dolostones. (a) Dark-grey massive dolostone (indicated by red arrows) interbedded with grey limestone (indicated by yellow arrows) (Maokou Formation, Panxian). (b) Dark-grey massive dolostone (indicated by red arrow) interbedded with grey limestone (indicated by yellow arrow) (Maokou Formation, Shilin). (c) Dark-grey massive dolostone interbedded with grey limestone (Maokou Formation, Xiaohuangpo). (d) Dark-grey massive dolostone with slash marks resulting from differential weathering (Machel, 2004) (Maokou Formation, Fanglecun). (e) Dark-grey massive dolostone interbedded with grey limestone (Maokou Formation, Shizong). (f) Dark-grey massive dolostone interbedded with grey limestone (Maokou Formation, Shuanglongcun).

dolomites are cut by stylolites (Fig. 9f). For patchy dolostones, the contact between dolomite patches and limestone patches is sharp; within the dolomite patches, the dolomite crystal size and shape showed no significant change (Fig. 9g, h).

Notably, the dolomites of some samples are mainly concentrated in two types of sites: (1) areas of relatively low micrite matrix content (Fig. 9g–i); and (2) intergranular and intragranular pores (Fig. 9j–l). In some samples, crescent-shaped calcite cements were

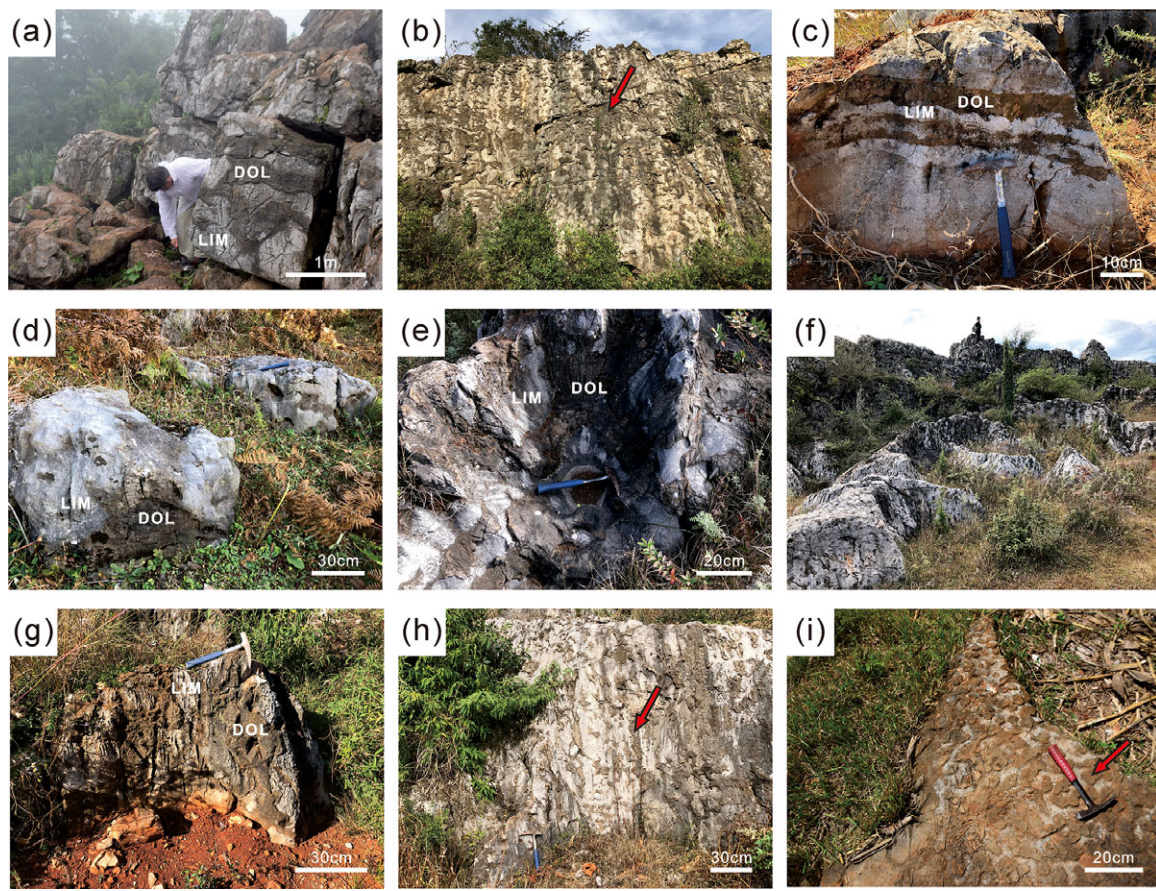


Fig. 7. (Colour online) Macroscopic characteristics of patchy dolostones. (a) Grey patchy dolostone, in which dolomite patches exhibit various shapes. The stratigraphic dip is 27° (Maokou Formation, Xishan). (b) Grey patchy dolostone, in which dolomite patches show darker colour (indicated by red arrow). The stratigraphic dip is 12° (Maokou Formation, Shuanglongcun). (c) Grey patchy limestone with parallel-elongated dolomite patches. The stratigraphic dip is 12° (Maokou Formation, Shuanglongcun). (d) Grey patchy limestone, in which dolomite patches show darker colour. The stratigraphic dip is 18° (Maokou Formation, Xiaohuangpo). (e) The inner structure of patchy dolostone, in which dolomite patches are grid-shaped. The stratigraphic dip is 12° (Maokou Formation, Shuanglongcun). (f) Dark-grey patchy dolostones (top) transitioning to grey patchy limestones (bottom). Dolomite patches are darker in colour. The stratigraphic dip is 12° (Maokou Formation, Shuanglongcun). (g) Grey patchy dolostones with vertically elongated dolomite patches. The stratigraphic dip is 12° (Maokou Formation, Shuanglongcun). (h) Grey patchy dolostones with vertically elongated dolomite patches (indicated by red arrow). The stratigraphic dip is 12° (Maokou Formation, Shuanglongcun). (i) The top surface of a patchy dolostone with vertically elongated dolomite patches (indicated by red arrow). The stratigraphic dip is 10° (Maokou Formation, Shilin).

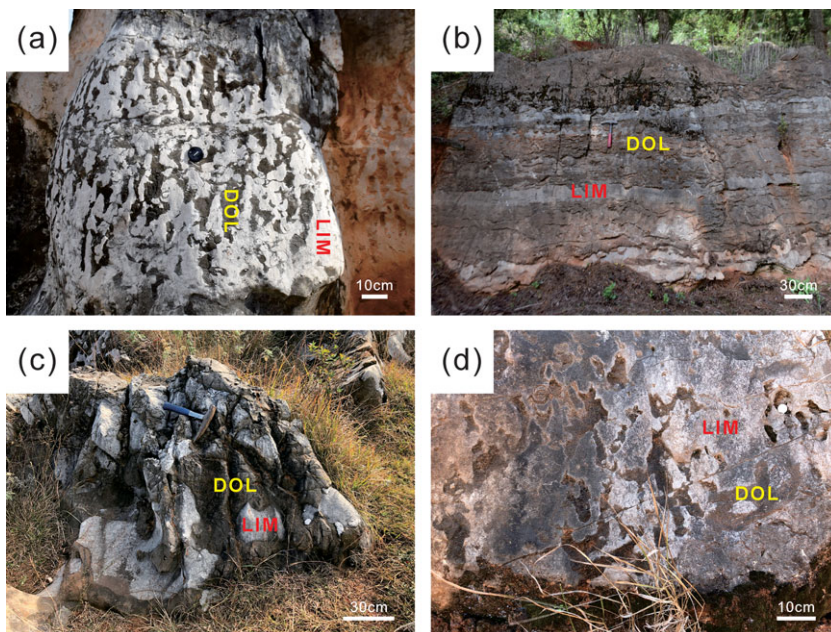


Fig. 8. (Colour online) Types of patchy dolostones/limestones. (a) Grey patchy limestones with vertically elongated dolomite patches. The stratigraphic dip is 10° (Maokou Formation, Shilin). (b) Grey patchy dolostones with parallel-elongated dolomite patches. The stratigraphic dip is 10° (Maokou Formation, Shilin). (c) Grey patchy dolostones, containing grid-shaped dolomite patches. The stratigraphic dip is 12° (Maokou Formation, Shuanglongcun). (d) Grey patchy limestones, containing irregularly shaped dolomite patches. The stratigraphic dip is 11° (Maokou Formation, Fenglegcun).

Table 1. Geochemical characteristics (average values) of massive and patchy dolostones

Dolostone type	Order degree	Homogenization temperature (°C)	Salinity (wt% NaCl eq)	$\delta^{13}\text{C}_{\text{PDB}}$ (‰)	$\delta^{18}\text{O}_{\text{PDB}}$ (‰)	$^{87}\text{Sr}/^{86}\text{Sr}$	$\delta^{26}/^{24}\text{Mg}$ (‰)
Massive	0.8984	172.31	5.75	3.83	-9.77	0.707967 ± 0.000018	-1.75 ± 0.03
Patchy	0.8439	166.88	5.26	3.81	-9.00	0.707654 ± 0.000017	-1.72 ± 0.03

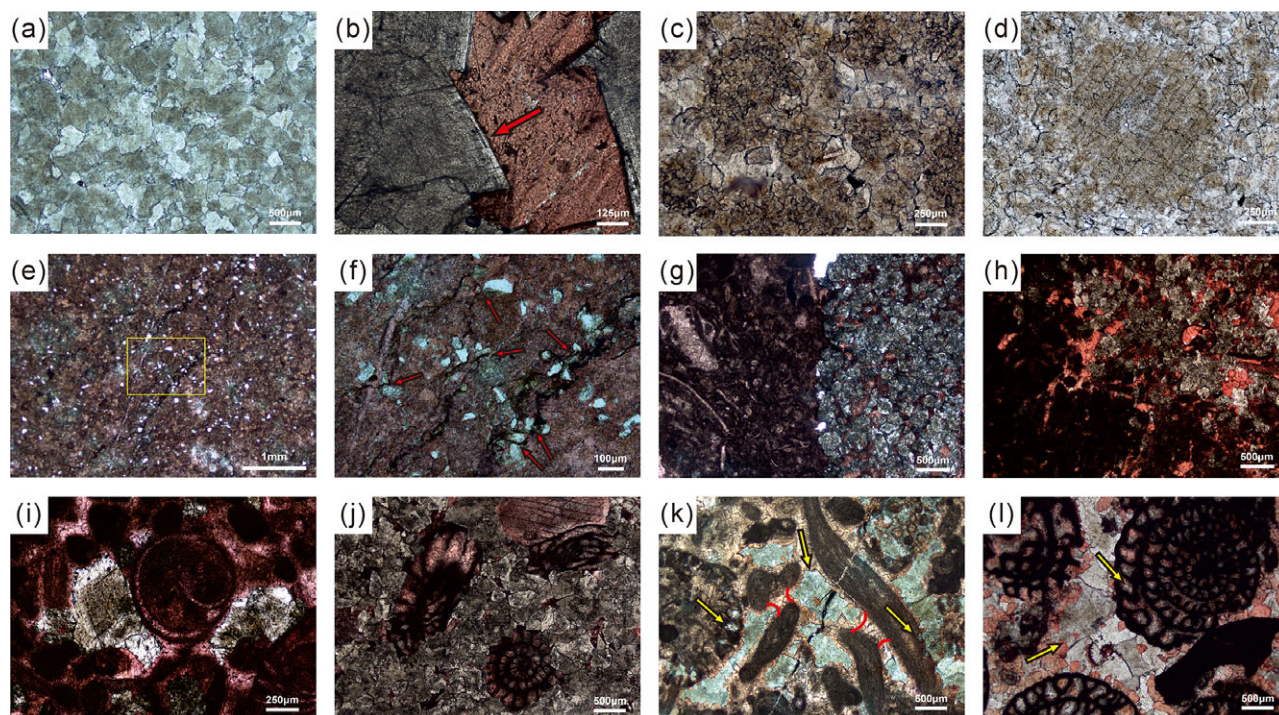


Fig. 9. (Colour online) Microscopic features of dolostones. (a) Dolostone with medium- to coarse-sized crystals. The crystal shapes are mainly planar-subhedral and nonplanar-anhedral; plane-polarized light (PPL) (Maokou Formation, Zhijin). (b) Saddle dolomite with medium-sized crystals. The crystal face is indicated by the arrow; the red colour indicates calcite. PPL (Maokou Formation, Shizong). (c) Dolostone in which original microstructural features from the limestone precursor are preserved. The crystals mainly contain fine-grained dolomites; PPL (Maokou Formation, Langdai). (d) Dolostone in which original microstructural (echinoderm) features from the limestone precursor are preserved. The crystals mainly contain fine- to medium-grained dolomites; PPL (Maokou Formation, Fenglecun). (e) Dolomites were scattered relatively evenly among the calcites, but were enriched near the stylolites; PPL (Maokou Formation, Miaotian). (f) Enlarged image delineated by the yellow box in (e), in which the dolomites are cut by stylolites (indicated by red arrows); PPL. (g) Dolomites developed preferentially in bioclastic grainstone areas of the rock. The crystals mainly contain fine-grained dolomites; PPL (Maokou Formation, Xishan). (h) Dolomites developed preferentially in areas with relatively low micrite matrix content. The crystals mainly contain fine-grained dolomites; PPL (Maokou Formation, Shilin). (i) Dolomites developed preferentially in areas with relatively low micrite matrix content. The crystals mainly contain medium- to coarse-grained dolomites; PPL (Maokou Formation, Hunshuitang). (j) Dolomites developed preferentially in intergranular areas. The crystals mainly contain medium-grained dolomites; PPL (Maokou Formation, Shizong). (k) Dolomites developed preferentially in intergranular pores and intragranular pores (indicated by yellow arrow). Crescent-shaped calcite cements centred in the grain contact area (indicated by red line). The crystals mainly contain medium- to coarse-grained dolomites; PPL (Maokou Formation, Zhijin). (l) Dolomites developed preferentially in intergranular and intragranular pores (indicated by yellow arrow). The crystals mainly contain medium- to coarse-grained dolomites; PPL (Maokou Formation, Langdai).

centred in grain contact areas and other calcite cements were found between dolomites and calcite grains (Fig. 9k, l).

4.c. Cathodoluminescence analysis

The general CL characteristics of the different dolomites in the study area are consistent, including weak CL intensity and relatively uniform CL colour, with the only subtle difference in specific CL colour such as dark red and deep purple. In contrast, the calcites did not exhibit luminescence (Fig. 10).

The dolomite crystals exhibit zonal structure, in which the crystal cores are mainly characterized by uniformly dark red (Fig. 10b, d, f, h, j, r, t) and deep purple (Fig. 10l, n, p) in CL, and the crystal edges (growth zones) show a stronger luminescence with brighter colour and less thickness (Fig. 10b, d, j, l, n, p, t).

In some samples, such as a sample of the Maokou Formation in Xiaohuangpo, dolomite crystals of different sizes show similar luminescence in CL (Fig. 10f). In other samples, such as those from the Maokou Formation in Xiaohuangpo and in Fenglecun, the CL intensities of the dolomites were generally weak but differed slightly in dolomites of different sizes; dolomites in which the original structure was preserved (echinoderms) exhibited relatively strong CL (Fig. 10h, t). Generally, brighter luminescence occurs in cleavage slits (Fig. 10t) and at crystal boundaries suffering from dissolution (Fig. 10p).

4.d. Order degree of dolomite

The order degree values for the dolomite crystals in the study area range from 0.7240 to 0.9976, with an average of 0.8892. Maokou

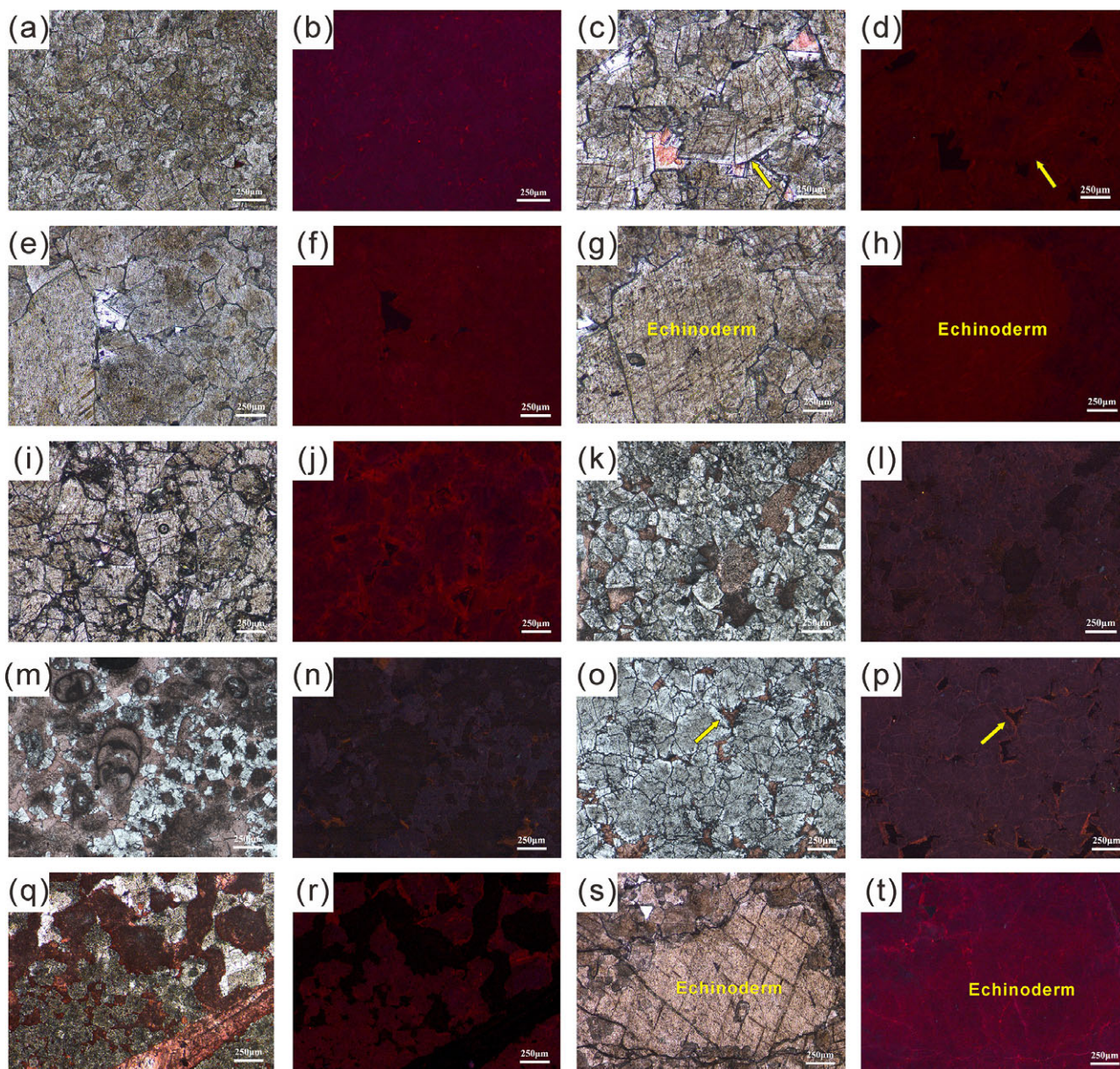


Fig. 10. (Colour online) CL of dolomite. (a) Dolostone of fine crystal size. The crystal shapes are mainly planar-subhedral and nonplanar-anhedral; PPL (Maokou Formation, Hunshuitang). (b) CL image corresponding to (a), in which the dolomites show weak CL. (c) Dolostone of fine to medium crystal size. The crystal shapes are mainly planar-subhedral. Saddle dolomites can be observed with warped crystal faces (indicated by arrow); PPL (Maokou Formation, Xiaohuangpo). (d) CL image corresponding to (c), in which the dolomite shows weak CL and the calcite does not show CL. (e) Dolostone of fine to medium crystal size. The crystal shapes are mainly planar-subhedral; PPL (Maokou Formation, Xiaohuangpo). (f) CL image corresponding to (e). (g) Dolostone of fine to medium crystal size. The crystal shapes are mainly planar-subhedral; PPL (Maokou Formation, Xiaohuangpo). (h) CL image corresponding to (g). (i) Dolostone of fine to medium crystal size. The crystal shapes are mainly planar-subhedral; PPL (Maokou Formation, Hunshuitang). (j) CL image corresponding to (i). (k) Dolostone of fine crystal size. The crystal shapes are mainly planar-subhedral and nonplanar-anhedral; PPL (Maokou Formation, Shuanglongcun). (l) CL image corresponding to (k). (m) Dolostone of powder to fine crystal size. The crystal shapes are mainly planar-euhedral and planar-subhedral; PPL (Maokou Formation, Shuanglongcun). (n) CL image corresponding to (m). (o) Dolostone of fine to medium crystal size. The crystal shapes are mainly planar-subhedral; PPL (Maokou Formation, Shuanglongcun). (p) CL image corresponding to (o). The dolomite crystal boundaries suffering from dissolution show brighter luminescence in CL (indicated by arrow). (q) Dolostone of fine to medium crystal size. The crystal shapes are mainly planar-subhedral and nonplanar-anhedral; PPL (Maokou Formation, Fenglecun). (r) CL image corresponding to (q). (s) Dolostone of fine to medium crystals. The crystal shapes are mainly planar-subhedral; PPL (Maokou Formation, Fenglecun). (t) CL image corresponding to (s).

Formation dolomite crystals and Qixia Formation dolomite crystals exhibit similar characteristics (Table 2).

4.e. Fluid inclusion analysis

Primary fluid inclusions of useful size for microthermometry (i.e. > 2 μm in diameter; Goldstein & Reynolds, 1994) were scattered throughout the dolomite crystals, and neither stretching nor

directionality was observed. These inclusions were two-phase inclusions, liquid-rich with a vapour bubble, colourless and transparent with clear boundaries and regular shapes. The inclusions ranged in size from 2.5 to 9 μm with an average of 4.7 μm (Fig. 11).

Homogenization temperatures of the fluid inclusions within dolostones range from 101 to 192°C (average, 169.52°C). The homogenization temperatures are mainly concentrated in the range of 164–185°C. Salinities of fluid inclusions within dolostones

Table 2. Order degree of middle Permian dolomite crystals in East Yunnan

Formation	Sampling section	No. of samples	Range/value	Average
Maokou	Xishan	1	0.9386	0.9386
	Fenglecun	15	0.7707–0.9781	0.8845
	Xiaohuangpo	5	0.9335–0.9976	0.9607
	Shilin	2	0.8451–0.9007	0.8729
	Hunshuitang	1	0.9657	0.9657
	Shizong	1	0.8353	0.8353
	Shuanglongcun	3	0.7240–0.7415	0.7343
	Zhijin	1	0.9505	0.9505
Qixia	Xishan	1	0.8603	0.8603

range from 4.49 to 8.41 wt% NaCl eq (average, 5.50 wt% NaCl eq). The salinities of fluid inclusions are mainly concentrated in the range of 4.49–5.59 wt% NaCl eq (Fig. 11).

Note that compared with patchy dolostones, massive dolostones have higher homogenization temperatures and salinities of fluid inclusions (Table 1; Fig. 12). Additionally, there is a slight linear relation between the salinity and homogenization temperature of fluid inclusions, such that the salinity increases with the temperature (Fig. 12).

Fluid inclusions within Maokou Formation dolostones and Qixia Formation dolostones exhibit similar characteristics (Table 3).

4.f. Carbon and oxygen isotope analysis

$\delta^{13}\text{C}_{\text{PDB}}$ values for dolomites in the study area range from 2.24 to 5.27‰ with an average of 3.82‰. The $\delta^{18}\text{O}_{\text{PDB}}$ values range from –6.31 to –13.75‰, with an average of –9.43‰ (Fig. 13). Note that, compared with patchy dolostones, massive dolostones have lower $\delta^{18}\text{O}_{\text{PDB}}$ values (Table 1; Fig. 13). The Maokou Formation dolostones and Qixia Formation dolostones show similar $\delta^{13}\text{C}_{\text{PDB}}$ and $\delta^{18}\text{O}_{\text{PDB}}$ characteristics (Table 4).

4.g. Strontium isotope analysis

$^{87}\text{Sr}/^{86}\text{Sr}$ values for dolomites in the study area range from 0.707354 to 0.708522 with an average of 0.707841. A total of five datasets of $^{87}\text{Sr}/^{86}\text{Sr}$ values for Permian seawater were collected to compare with those of the dolostones in East Yunnan. The first three datasets were obtained from the Yangtze platform (Lu *et al.* 1992; Huang, 1997; Huang *et al.* 2001), and the remaining data were obtained from elsewhere in the world (McArthur *et al.* 2001; Korte *et al.* 2006). Notably, these five datasets show similar $^{87}\text{Sr}/^{86}\text{Sr}$ ranges for the Permian seawater. However, the $^{87}\text{Sr}/^{86}\text{Sr}$ values for middle Permian seawater from the first three datasets (Yangtze platform) are higher than those from the latter two datasets (Table 5).

4.h. Magnesium isotope analysis

$\delta^{26}\text{Mg}_{\text{DSM3}}$ values for dolomites in the study area range from –0.91 to –2.12‰, with an average of –1.74‰. Notably, the $\delta^{26}\text{Mg}_{\text{DSM3}}$ values for dolomites in the study area gradually decrease from the inner belt to the outer belt of the active area of the Emei mantle plume (Fig. 14; Table 6).

5. Discussion

5.a. Characteristics of dolomitizing fluid

The massive dolostones and patchy dolostones are of the same origin, with the only difference being the degree of dolomitization (Table 1). The homogenization temperatures and salinities of fluid inclusions within the dolostones, the petrographic characteristics of the dolostones, and the carbon and oxygen isotopic characteristics of the dolostones all indicate that the dolomitization fluid was of high temperature and moderate salinity.

The homogenization temperature of the fluid inclusions within the dolostones is generally greater than 101°C (Fig. 11), indicating that the dolomitization fluid was a high-temperature fluid that broke through the dynamic barrier to form the dolomite (Warthmann *et al.* 2000; Wright & Wacey, 2004).

The salinities of the fluid inclusions within the dolostones range from 4.49 to 8.41 wt% NaCl eq, with an average of 5.50 wt% NaCl eq (Fig. 11), indicating that the dolomitization fluid was of moderate salinity.

Petrography reveals the dolomite crystals to be fine to coarse sized. The crystal shapes of the dolostones are mainly planar-subhedral, nonplanar-anhedral and nonplanar-saddle (Fig. 9); these shapes also indicate that the dolomites were formed by relatively high-temperature fluids (Shukla *et al.* 1984; Machel, 2004).

$\delta^{18}\text{O}_{\text{PDB}}$ values of the dolomites are negative (Fig. 13), which is mainly attributed to the high-temperature effect (Vasconcelos *et al.* 2005; Sharp, 2007), consistent with the analysis of the fluid inclusions.

In addition, $\delta^{13}\text{C}_{\text{PDB}}$ values of the dolomites are high, mostly above 3‰. These values are similar to the carbon isotope signatures of other marine carbonates deposited during the same period (Fig. 13) (Huang, 1997; Veizer *et al.* 1999; Huang & Zhou, 2010). This similarity indicates that the carbon in the dolomites mainly originates from the dissolution of local calcite and/or aragonite. The high $\delta^{13}\text{C}_{\text{PDB}}$ values are attributed to the high-speed burial of organic matter during this period (Huang, 1997).

Calcite in the study area is non-luminescent in CL, indicating that it is the primary marine carbonate mineral with low manganese, with the diagenetic fluid possibly being seawater. The ferroan dolomite in the study area is rare and the dolomite shows weak CL, indicating that the dolomite was less affected by non-marine fluids and formed in reducing environments (Machel, 1985; Huang, 1992; Gillhaus *et al.* 2001) (Fig. 10). The dolomite crystals are characterized by zonal structures, indicating that they have undergone multi-stage diagenesis of at least two stages (Fig. 10). The initial dolomites (crystal cores) formed by replacement are characterized by a relatively uniform CL colour, indicating that the diagenetic environment in the early stage was relatively stable; the latter dolomite cements (crystal edges) demonstrate a stronger luminescence with a brighter CL colour and a lesser thickness, indicating that the dolomitization fluid composition and dolomite crystallization rate varied in the latter stage, while the action time was relatively short (Fig. 10).

In some samples (Fig. 10f) dolomite crystals of different sizes exhibit the same luminescence in CL, indicating that their dolomitization fluids were the same. In contrast, in other samples (Fig. 10h, t) dolomite crystals of different sizes exhibit slightly different luminescence intensity in CL, with dolomites that preserved the original structure (echinoderm) showing relatively strong CL. This is not due to different dolomitizing fluids, but because the original mineral phases of dolomites are different (Huang, 1990). The brighter luminescence in cleavage slits and crystal

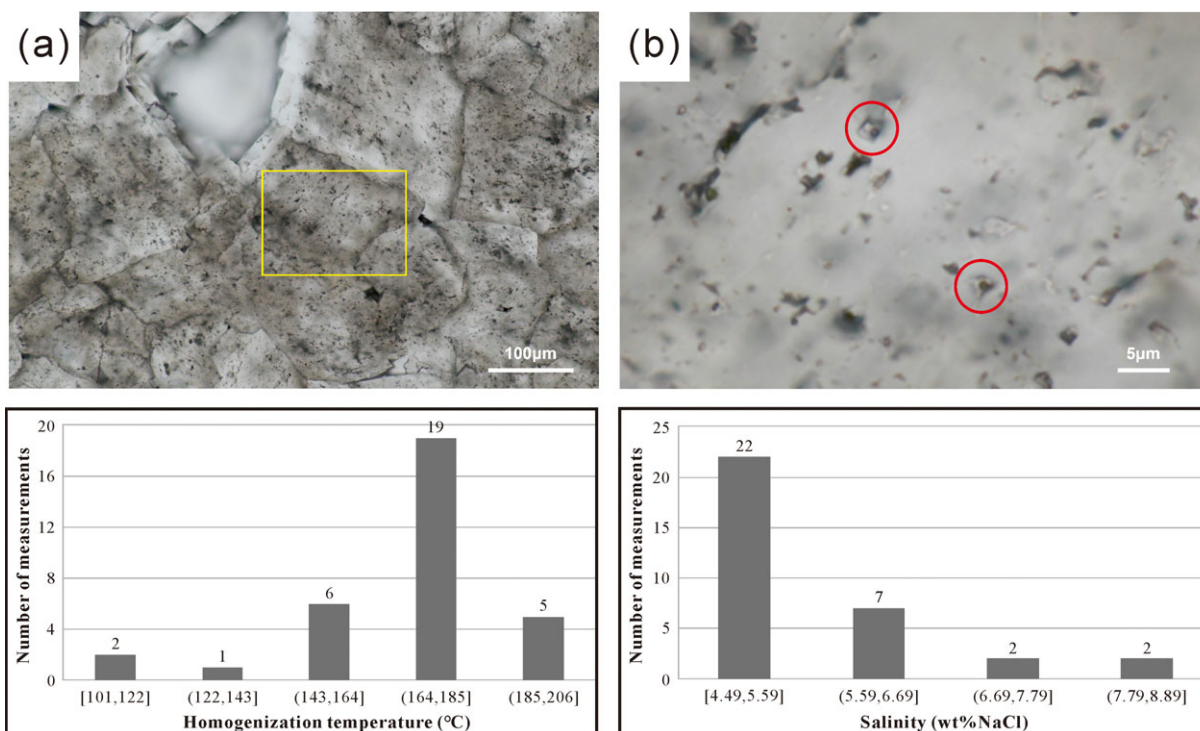


Fig. 11. (Colour online) Fluid inclusion features and histograms of homogenization temperatures and fluid inclusion salinities for middle Permian dolostones of East Yunnan. (b) Enlarged image delineated by the yellow box in (a). Fluid inclusions are indicated by red circles.

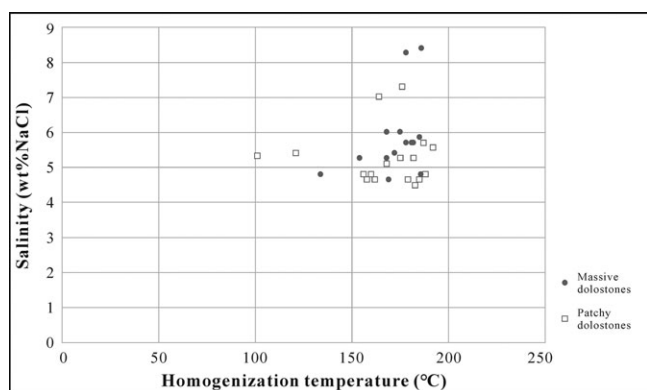


Fig. 12. Scatter diagram of homogenization temperatures and fluid inclusion salinities for middle Permian dolostones of East Yunnan.

boundaries suffering from dissolution suggests that late-stage fluids interacted with the dolomite and that their properties were different from the early dolomitizing fluids (Fig. 10p, t).

5.b. Origin of dolomitizing fluid

On the basis of the above, the dolomitizing fluid in the study area should have the following characteristics: (1) high temperature; (2) moderate salinity; (3) abundant in Mg²⁺; and (4) a long-term, sustainable and active hydrological driving mechanism. This last expectation is based on the region’s large geographic and volumetric scale of dolostone, requiring a substantial quantity of dolomitizing fluid.

Currently, the main formation mechanisms of dolostone include the microbial/organogenic model, sabkha model, seepage

reflux model, mixing zone model, hydrothermal dolomitization, compaction model, tectonic (squeegee) model, topography-driven model and thermal convection model (Machel, 2004).

The crystals of the dolostones in the study area ranged from fine to coarse (Fig. 9), which is much larger than that predicted by the microbial/organogenic model (typically < 10 μm) (Vasconcelos & McKenzie, 1997; Warthmann *et al.* 2000; Hu *et al.* 2014). The origin of the dolomitizing fluid therefore cannot be explained by the microbial/organogenic model.

The order degree of dolomite is relatively high in the study area (Table 2). Compared with previous research (Huang, 1985; Zeng & Wan, 2004, Zhang *et al.* 2014), the order degree of dolomite in the study area is significantly higher than that predicted by the sabkha model, seepage reflux model or mixing zone model (mean value, 0.59–0.67). In addition, the dolomitizing fluid in the study area had a high temperature; the origin of the dolomitizing fluid therefore cannot be explained by the sabkha, seepage reflux or mixing zone models (Zenger & Dunham, 1980; Machel, 2004).

A hydrothermal model would seem to better fit these order degrees and temperature expectations. However, the dolostones of the study area rarely exhibit typical characteristics of hydrothermal dolostone, such as: zebra texture (in which dark matrix dolomite bands alternate with bands of white saddle dolomite) (Machel, 2004); milky white colour with a pearly luster in hand specimens; intercrystalline holes that are filled with hydrothermal minerals; or being strictly controlled by basement faults (Machel, 2004). Additionally, the salinities of fluid inclusions within dolostones in the study area are significantly lower than those of the hydrothermal fluid in the study area (15–24 wt% NaCl) (Li *et al.* 2011; Hou *et al.* 2013). The dolomitizing fluid was therefore not a deep hydrothermal fluid, and the dolostone in the study area does not belong to this class of structurally controlled hydrothermal dolostone.

Table 3. Homogenization temperatures and fluid inclusion salinities for middle Permian dolostones of East Yunnan

Formation	Sampling section	No. of inclusions	Homogenization temperature (°C)		Salinity (wt% NaCl eq)	
			Range/value	Average	Range/value	Average
Maokou	Xishan	6	168–186	172.67	4.65–5.41	5.03
	Fenglecun	6	178–188	183.17	4.49–8.41	5.88
	Xiaohuangpo	1	134	134	4.8	4.8
	Shilin	4	168–182	175.25	5.11–7.31	5.74
	Shizong	7	154–185	174.71	5.26–6.01	5.75
	Shuanglongcun	1	121	121	5.41	5.41
	Zhijin	2	187–192	189.5	5.56–5.71	5.64
Qixia	Hunshuitang	5	156–164	160	4.65–7.02	5.18
	Shuanglongcun	1	101	101	5.33	5.33

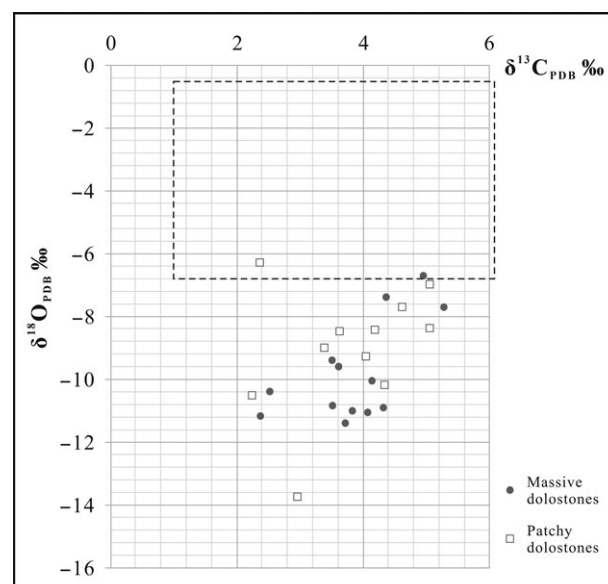
Table 4. Carbon and oxygen isotope data for middle Permian dolostones in East Yunnan

Formation	Sampling section	No. of samples	$\delta^{13}\text{C}_{\text{PDB}}$ average (‰)	$\delta^{18}\text{O}_{\text{PDB}}$ average (‰)
Maokou	Xishan	1	4.345	−10.189
	Fenglecun	5	3.218	−9.970
	Xiaohuangpo	4	3.955	−10.711
	Shilin	3	3.641	−7.374
	Hunshuitang	2	3.895	−11.236
	Shizong	2	2.603	−12.14
	Shuanglongcun	3	5.025	−7.352
Qixia	Xishan	2	4.005	−8.364
	Hunshuitang	2	3.514	−8.735

Burial compaction (compaction model) and tectonically induced flow (tectonic (squeeze) model) can generate only limited amounts of dolostone; the former involves a limited volume of compaction water and the latter involves a short-lived squeeze-type flow system with low flux (Machel & Anderson, 1989; Deming *et al.* 1990; Amthor *et al.* 1993; Machel *et al.* 2000; Buschkuehle & Machel, 2002; Machel, 2004). The origin of the dolomitizing fluid therefore cannot be explained by these two models.

The dolomitizing fluid of the topography-driven model is meteoric water, which dissolves enough Mg^{2+} en route before encountering limestone (Tóth, 1988; Machel, 2004). Although the Emei basalt covering the Maokou Formation is rich in Mg^{2+} (4.5–6.51%) (Meade, 2010), causing some researchers to hypothesize that the Mg^{2+} of the dolomitizing fluid originated from this basalt (Jin & Feng, 1999), the $^{87}\text{Sr}/^{86}\text{Sr}$ values for the dolomites in the study area are significantly higher than those of the Emei basalt ($^{87}\text{Sr}/^{86}\text{Sr}$ value, 0.7045–0.7065) (Mao, 1991; Jiang *et al.* 2014). The topography-driven model therefore cannot explain the origin of the dolomitizing fluid.

We believe that the dolomitization in the study area must be modelled as an open thermal convection mechanism (Raffensperger & Vlassopoulos, 1999). Thermal convection would be driven by spatial variations in temperature caused by elevated heat flux in the vicinity of

**Fig. 13.** (Colour online) Carbon and oxygen isotope data for middle Permian dolostones in East Yunnan. The dashed-line box represents the $\delta^{13}\text{C}_{\text{PDB}}$ and $\delta^{18}\text{O}_{\text{PDB}}$ ranges for the middle Permian low-Mg calcitic shells (Veizer *et al.* 1999).

the Emei mantle plume. This convection would result in changes in pore-water density and thus produce an effective hydraulic head (Machel, 2004). Open convection cells would form in carbonate platforms that were open to seawater recharge and discharge at the top. The dolomitizing fluid would be mostly seawater, with a minor contribution from deep hydrothermal fluid driven by the Emei mantle plume. The evidence for this hypothesis is discussed in the following.

First, the difference between the $^{87}\text{Sr}/^{86}\text{Sr}$ values for middle Permian seawater and the Yangtze platform and elsewhere in the world (Table 5) can be explained using the influence of the Yunnan movement that occurred at the end of the Carboniferous Period (Zhou *et al.* 2005; Su *et al.* 2015). As a result of the Yunnan movement that occurred in southern China during the latter part of the Carboniferous Period, the Yangtze platform was uplifted and suffered strong denudation, resulting in a regional unconformity between middle Permian and Carboniferous rocks and the absence of lower Permian strata in the Yangtze platform. At this time, the amount of exposed land area drastically expanded,

Table 5. Comparison of strontium isotope data between middle Permian dolostones and Permian seawater

Sampling section	$^{87}\text{Sr}/^{86}\text{Sr}$	Standard error
Xiaohuangpo	0.708522	0.000016
Fenglecun	0.707783	0.000011
Fenglecun	0.707473	0.00002
Fenglecun	0.707716	0.000021
Shilin	0.707762	0.000017
Shilin	0.708506	0.000026
Shuanglongcun	0.707837	0.000017
Shuanglongcun	0.707354	0.00002
Hunshuitang	0.707590	0.000013
Zhijin	0.707871	0.000016
Permian/middle Permian seawater	0.70672–0.70821/0.70730–0.70821 (Lu <i>et al.</i> 1992)	
	0.70589–0.70868/0.70589–0.70868 (Huang, 1997)	
	0.70672–0.70821/0.70730–0.70821 (Huang <i>et al.</i> 2001)	
	0.70690–0.70820/0.70690–0.70762 (McArthur <i>et al.</i> 2001)	
	0.70684–0.70817/0.70684–0.70747 (Korte <i>et al.</i> 2006)	

and more crustal-source Sr (rich in ^{87}Sr) accumulated in strata (Zhou *et al.* 2005; Chen *et al.* 2011; Su *et al.* 2015). During the early part of the middle Permian, the transgression occurred, and this crustal-source Sr was released from rocks and introduced into the ocean, causing the middle Permian seawater of the Yangtze platform and the carbonate rocks formed during this period to have higher $^{87}\text{Sr}/^{86}\text{Sr}$ values.

Most of the $^{87}\text{Sr}/^{86}\text{Sr}$ values for the dolomites in the study area were therefore within the ranges for Permian or middle Permian seawater in the Yangtze platform (Table 5). This similarity suggests that the Permian seawater of the Yangtze platform (rich in Mg^{2+}) is the primary candidate for the dolomitizing fluid in the study area.

Only two dolomite data points exceed the $^{87}\text{Sr}/^{86}\text{Sr}$ range for Permian seawater (Table 5), which is assumed to be influenced by some external factors such as deep hydrothermal fluids passing through the aluminosilicate basement rocks.

Second, the carbonate platform in the study area was underlain by a mantle plume, which can result in particularly fast and pervasive dolomitization and would have provided a lasting and active hydrologic driving mechanism.

Third, the high temperature of the dolomitizing fluid can be explained by the activity of the Emei mantle plume. Based on their burial history and geothermal features (Wang *et al.* 1986; Yuan *et al.* 2006; Wo *et al.* 2007; Huang *et al.* 2014; Jiang *et al.* 2014; Tian *et al.* 2014; Hao *et al.* 2015), the dolostones in the study area were clearly affected during dolomitization by high-temperature thermal events, likely related to the Emei mantle plume.

Fourth, the moderate salinity of the dolomitizing fluid was likely to the result of the mixing of seawater and deep hydrothermal fluid driven by the Emei mantle plume during thermal convection. The Permian seawater of the Yangtze platform, which has a

Table 6. Magnesium isotope data for middle Permian dolostones in East Yunnan

Sampling section	$\delta^{26/24}\text{Mg}$ (‰)	2 × standard error
Xiaohuangpo	−0.91	0.03
Xiaohuangpo	−1.06	0.02
Fenglecun	−1.97	0.02
Fenglecun	−1.98	0.01
Shilin	−2.12	0.04
Shuanglongcun	−2.00	0.02
Hunshuitang	−2.12	0.04

low salinity of 4.4 wt% NaCl (Chen *et al.* 2013), is the primary candidate for the dolomitizing fluid; the hydrothermal fluid, which has a high salinity of 15–24 wt% NaCl (Li *et al.* 2011; Hou *et al.* 2013) is the secondary candidate. In some areas, the proportion of hydrothermal fluid could be higher, so that the saddle dolomites can be formed (but the overall number is very low). The salinity slightly increased linearly with the homogenization temperature for these fluid inclusions (Fig. 12). This is probably because the temperature and hydrothermal component of the dolomitizing fluids is higher in regions showing more intense plume activity, such that the salinity of the fluids is also higher.

Fifth, the dolomitization of the study area was selective. From a macroscopic perspective, the dolostones are mainly distributed in the Maokou Formation, which is dominated by bioclastic grainstone. Further, the Qixia Formation, which is dominated by bioclastic packstone, does not exhibit obvious dolomitization (Fig. 4). From a microcosmic perspective, dolomitization appears to have been initiated at sites with relatively low micrite matrix contents (i.e. high primary porosity and permeability), as shown in Figure 9g–i, and at sites of intergranular pores and intragranular pores, which are mainly primary pores as shown in Figure 9j–l. In some samples, crescent-shaped calcite cements were centred in the grain contact areas (Fig. 9k); these were likely formed when the limestone experienced a freshwater vadose environment (James & Choquette, 1984). Furthermore, in some samples, such as that shown in Figure 9k, calcite cements were found between dolomites and calcite grains. All of these characteristics indicate that the limestone was buried (though not very deep) and underwent diagenesis before dolomitization (see details in Section 5.c). If the limestone was not buried before dolomitization, the bioclastic packstone would have a relatively high primary porosity and permeability similar to that in bioclastic grainstone (i.e. the difference is not obvious). If the limestone was buried deeply before dolomitization, the porosity and permeability of the bioclastic grainstone and bioclastic packstone would be very low as a result of diagenesis (Longman, 1980). In both cases, the dolomitization of the study area would not be selective. Before dolomitization, the porosity and permeability of the bioclastic packstone were therefore low, whereas those of the bioclastic grainstone were high enough to allow thermal convection.

From the inner belt to the outer belt of the active area of the Emei mantle plume, the temperature gradient would have gradually decreased, causing thermal convection to gradually weaken such that the thickness of dolostone (i.e. dolomitized rocks in that carbonate sequence) would gradually have decreased (Fig. 5). In addition, compared with patchy dolostones, massive dolostones

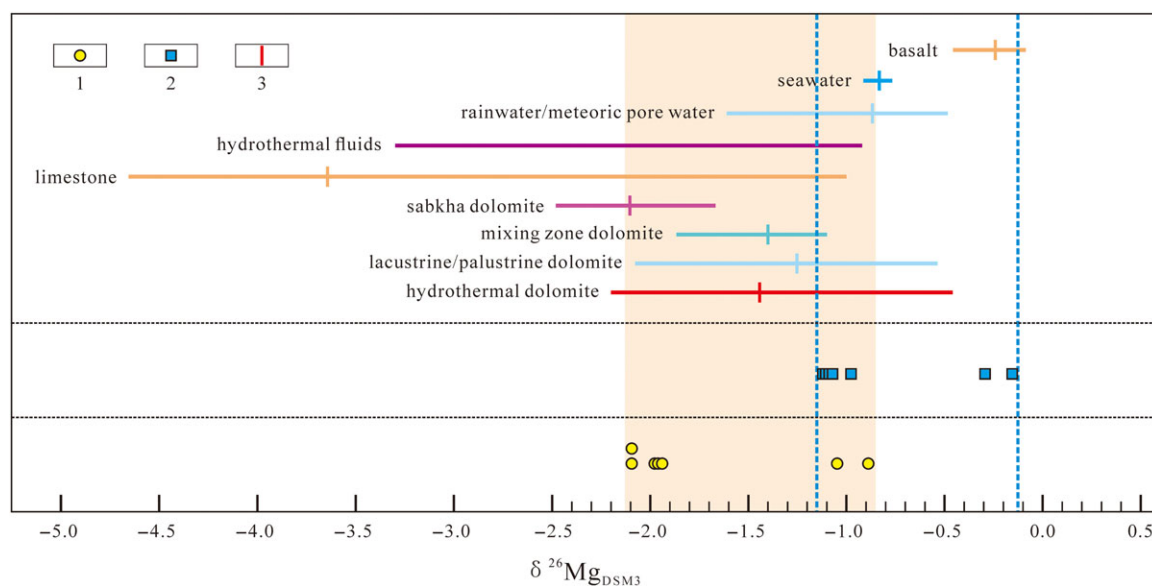


Fig. 14. (Colour online) Magnesium isotopic composition ($\delta^{26}\text{Mg}_{\text{DSM3}}$) of different Mg sources (Geske *et al.* 2015). 1, Magnesium isotope data for middle Permian dolostones in East Yunnan. 2, $\delta^{26}\text{Mg}_{\text{DSM3}}$ values calculated from the fractionation formula for dolomite precipitation (Li *et al.* 2015). 3, Average value of different Mg sources (Geske *et al.* 2015).

(which indicate relatively strong thermal convection) have higher average homogenization temperatures and fluid inclusions with greater salinities and lower $\delta^{18}\text{O}_{\text{PDB}}$ average values (Table 1; Figs 12, 13); these observations can also be explained by the open thermal convection model.

Sixth, the distribution and morphological characteristics of East Yunnan dolostones can be explained by the open thermal convection model (see details in Section 5.d). The predictions of this model can also be used to effectively interpret the CL characteristics of East Yunnan dolostones.

Seventh, during the active stage of the Emei mantle plume during the late middle Permian – early late Permian period, the entire Yangtze platform was uplifted; we therefore believe that the palaeogeography of the upper Permian strata reflects the differences in the degree of crustal uplift (i.e. the differences in the intensity of the Emei mantle plume activity). For instance, the terrestrial sedimentary settings indicate relatively strong activity of the Emei mantle plume, whereas the marine sedimentary settings indicate relatively weak Emei mantle plume activity (Fig. 3).

The thickness of dolomitized rocks closely correlates with the activity intensity of the Emei mantle plume (Fig. 5). It is therefore also likely that the thickness of dolomitized rocks has an indirect relation with the palaeogeography of the upper Permian strata. The palaeogeography of the upper Permian strata may therefore indicate that the dolomitization in this area is related to the mantle plume.

Eighth, a previous study concluded that dolomites lack typical $\delta^{26}\text{Mg}$ signatures characterizing their specific environment of dolomitization precipitation (Geske *et al.* 2015). In addition, $\delta^{26}\text{Mg}$ values for Permian seawater are lacking and no related literature exists for reference. Our $\delta^{26}\text{Mg}$ data are therefore difficult to utilize when interpreting the origin of dolomitizing fluid. The $\delta^{26}\text{Mg}_{\text{DSM3}}$ values of the dolomites gradually decrease from the inner belt to the outer belt of the active area of the Emei mantle plume (Fig. 14; Table 6), presumably because the influence of upper mantle fluids decreases away from the plume. If anything, this $\delta^{26}\text{Mg}_{\text{DSM3}}$ pattern also indicates that the dolomitization in

this area is likely to be related to the mantle plume and mantle-driven fluids.

5.c. Age of dolomitization

The dolostones in the study area were clearly affected during dolomitization by high-temperature thermal events related to the Emei mantle plume (Wang *et al.* 1986; Yuan *et al.* 2006; Wo *et al.* 2007; Huang *et al.* 2014; Jiang *et al.* 2014; Tian *et al.* 2014; Hao *et al.* 2015). The age of dolomitization therefore cannot be estimated from the homogenization temperature of the fluid inclusions. The high-temperature thermal events related to the Emei mantle plume began during the late middle Permian period. The dolomitization should therefore be of late middle Permian age.

The dolomitization model in the study area is a thermal convection model, with selective dolomitization. During dolomitization, the porosity and permeability of strata (bioclastic grainstone) were still high enough to sustain viable thermal convection cells. Previous studies have found that open thermal convection is active to a burial depth of about 2–3 km, provided that the sequence does not contain effective aquitards. Below 2–3 km of burial depth, compaction has reduced porosity and permeability to levels that are too low to sustain viable convection cells (Machel, 2004). This mechanism therefore indicates an estimated dolostone burial depth of no more than 2–3 km.

In some microscopic samples, scattered dolomites were relatively evenly distributed among the calcites but enriched near the stylolites (Fig. 9e), and the dolomites were cut by stylolites (Fig. 9f). It could be that the pressure solution caused the calcites to dissolve, resulting in the enrichment of dolomites (which are not easy to dissolve) near the stylolites (Wang *et al.* 2017). These phenomena indicate that the dolomitization appeared before the pressure solution; the burial depth of dolostones is therefore no more than 600–1000 m (Lind, 1993; Fabricius, 2000, p. 177–190; Machel, 2004).

The middle Permian strata of East Yunnan is 150–700 m thick (Ministry of Geology and Mineral Resources of PR China, 1982, p. 164–165), meeting the burial depth requirements described

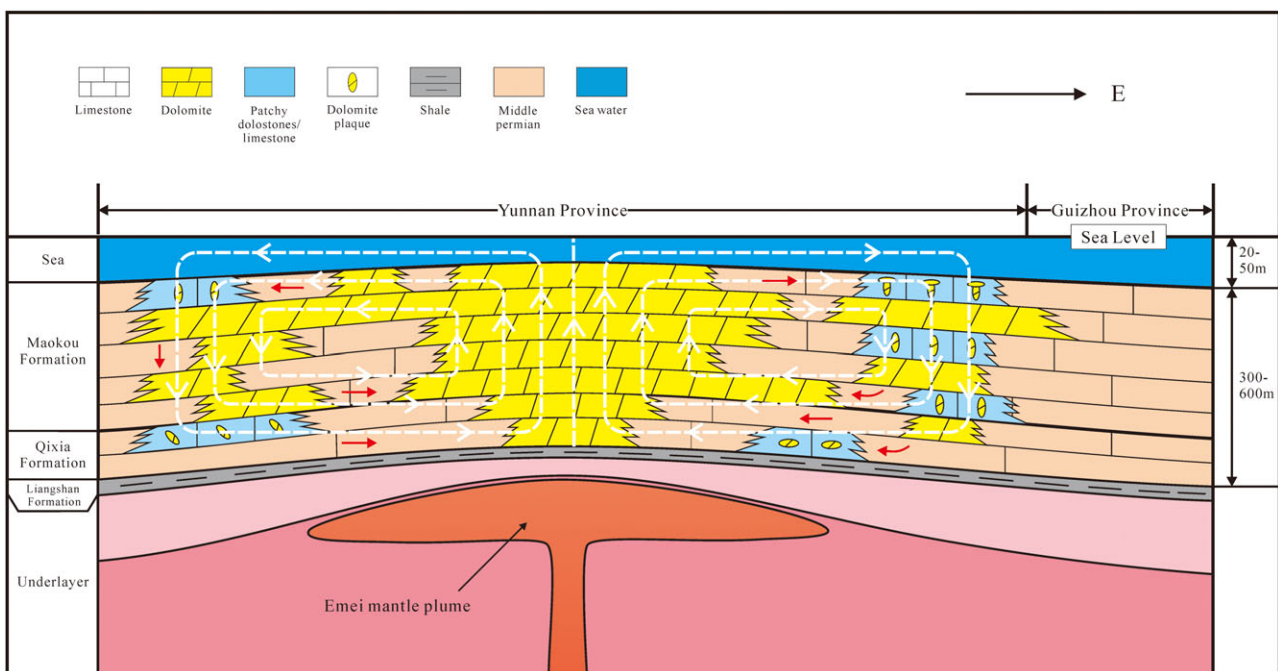


Fig. 15. (Colour online) Dolomitization model during the middle Permian period in East Yunnan. White dashed lines represent thermal convection flow pathways. Red solid lines represent flow pathways controlled by faults and fracture systems formed during the Dongwu movement.

above. In conclusion, the dolomitization in the study area should have occurred between the end of the middle Permian period at 259 Ma, and the initial basalt eruption period at 257 Ma (after the eruption, basalt covered the middle Permian rocks such that the carbonate platforms could not open to seawater) (Guo *et al.* 2004; He *et al.* 2007; Liu & Zhu, 2009; Li *et al.* 2012; <http://www.stratigraphy.org/index.php/ics-chart-timescale>).

5.d. Migration characteristics of dolomitizing fluid

5.d.1. Migration pathway

Previous studies have concluded that the magnitude and distribution of permeability are the most important parameters governing flow and dolomitization in an open thermal convection model (Kohout *et al.* 1977, p. 1–34; Simms, 1984; Kaufman, 1994; Sanford *et al.* 1998; Wilson *et al.* 2001; Whitaker *et al.* 2002, 2003, 2004, p. 99–139). As stated above, open thermal convection (Kohout convection) is active to a depth of about 2–3 km, providing that the sequence does not contain effective aquitards.

In the middle Permian limestone strata of East Yunnan, pores in bioclastic grainstone are the most important pathways for fluid migration. The distribution and microscopic characteristics of these dolostones (Figs 4, 9) indicate that dolostone development was closely related to the sedimentary setting: the host rocks of the dolostones are mainly bioclastic grainstone (shoal facies). Bioclastic grainstone has high porosity and permeability, which can provide pathways for fluid migration. The Maokou Formation contains the strongest development of middle Permian shoal facies; dolostones are therefore mainly distributed in the Maokou Formation.

In addition, the faults and fractures that formed during the Dongwu movement are also important migration pathways. They connect different shoal bodies such that the dolomitizing fluid can travel longer distances not only horizontally, but also vertically from one shoal body to another.

5.d.2. Driving force for migration

The open thermal convection of the study area was driven by spatial variations in temperature. These variations, caused by elevated heat flux in the vicinity of the Emei mantle plume, resulted in changes in pore-water density and thus produced an effective hydraulic head (Machel, 2004).

As a result of the influence of abnormally high temperatures resulting from Emei mantle plume activity, convective fluxes substantially increased, resulting in particularly fast and pervasive dolomitization (Combarnous & Bories, 1975; Wood & Hewett, 1982; Phillips, 1991).

5.d.3. Migration direction

By integrating all observed characteristics of the dolostone in the study area, particularly macroscopic characteristics, this study interprets the following circulation flow pathways for the dolomitizing fluid (Fig. 15).

In the horizontal plane, the driving force for thermal convection decreased away from the Emei mantle plume. The thickness of dolomitized rocks therefore gradually decreases from the inner belt to the outer belt of the active area of the Emei mantle plume (Fig. 5).

Vertically, the shape characteristics of dolomite patches suggest the direction of fluid migration (Figs 7, 8). Patchy dolostone/limestone with vertically elongated dolomite patches mainly exists in the vertical-flow region of thermal convection (i.e. when the direction of fluid was perpendicular to the bed plane). Patchy dolostone/limestone with parallel-elongated dolomite patches mainly occurs in the horizontal-flow region of thermal convection (i.e. when the direction of fluid was parallel to the bed plane). Patchy dolostone/limestone with grid-shaped dolomite patches or irregularly shaped dolomite patches mostly exists in the curved-flow region of thermal convection (i.e. when the direction of fluid was oblique to the bed plane). The mudstone of the

Liangshan Formation would have prevented the fluid from migrating downwards (Fig. 15).

5.e. Establishment of dolomitization model

We propose a mantle-plume-induced dolomitization model: open thermal convection dolomitization (Fig. 15). In this model, the Mg^{2+} of dolimitizing fluids mostly originates from seawater, with a minor component from deep hydrothermal fluid. The fluid moves along circulation flow pathways driven by spatial variations in temperature, resulting in large-scale dolomitization.

The dolomitizing fluid mainly migrates through the pores in bioclastic grainstone; the depositional setting of the dolostone is therefore as expected, that is, mainly shoal facies. The Maokou Formation in the study area is dominated by bioclastic grainstone and the water is relatively shallow; it is therefore the main locus for dolomitization in the middle Permian strata of East Yunnan.

This model explains the characteristics and distribution of dolostones in the study area; it can also be used to predict dolostone distributions in other areas subjected to thermal convection.

6. Conclusions

The main conclusions of this study are as follows.

1. The formation mechanism for the middle Permian dolostones in East Yunnan is open thermal convection dolomitization. Mg^{2+} in dolimitizing fluids predominantly originated from seawater, with a minor contribution from deep hydrothermal fluid.
2. The dolomitizing fluid mainly migrates through pores in bioclastic grainstone (shoal facies) and faults and fracture systems. Driven by spatial variations in temperature (due to elevated heat flux in the vicinity of the Emei mantle plume), the fluid migrates along the circulation flow pathways, resulting in fast and pervasive dolomitization of Middle Permian limestone.
3. The dolostones that have undergone open thermal convection dolomitization are mainly distributed in the Maokou Formation, which primarily contains shoal facies.

Finally, it is necessary to note that the dolomitization model proposed in this study is a concise and idealized model with a single hotspot (Emei mantle plume). However, the actual geological conditions of East Yunnan (700 km in diameter) must be much more complex than those of the proposed model. There could be some small secondary hotspots in the active area of the Emei mantle plume, which can also affect the composition and migration of the dolomitizing fluid. The elucidation of the specific impacts of these small secondary hotspots on dolomitization requires more experimental data and further studies in the future.

Acknowledgements. This research project was funded by the China National Petroleum Corporation (grant no. XNS14KS2016-040), the Sinopec Group (grant no. 34450000-15-ZC0607-0015) and the National Natural Science Foundation of China (grant no. 41872108). We thank the reviewer Theodore Present (Caltech) and an anonymous reviewer, whose useful suggestions and constructive criticisms helped to improve the manuscript. We thank Shuo Yi for her help with sample analysis. We also thank Enago for assistance with language.

Conflict of interest. None.

References

- Adams JE and Rhodes ML (1960) Dolomitization by seepage refluxion. *AAPG Bulletin* **44**, 1912–20.
- Amthor JE, Mountjoy EW and Machel HG (1993) Subsurface dolomites in Upper Devonian Leduc Formation buildups, central part of Rimbey-Meadowbrook reef trend, Alberta, Canada. *Bulletin of Canadian Petroleum Geology* **41**, 164–85.
- Anderson GM and Garven G (1987) Sulfate-sulfide-carbonate associations in Mississippi valley-type lead-zinc deposits. *Economic Geology* **82**, 482–8.
- Badiozamani K (1973) The dorag dolomitization model-application to the Middle Ordovician of Wisconsin. *Journal of Sedimentary Research* **43**, 965–84.
- Burns SJ, McKenzie JA and Vasconcelos C (2000) Dolomite formation and biogeochemical cycles in the Phanerozoic. *Sedimentology* **47**, 49–61.
- Buschkuehle BE and Machel HG (2002) Diagenesis and paleofluid flow in the Devonian Southesk-Cairn carbonate complex in Alberta, Canada. *Marine and Petroleum Geology* **19**, 219–27.
- Cervato C (1990) Hydrothermal dolomitization of Jurassic-Cretaceous limestones in the southern Alps, Italy: relation to tectonics and volcanism. *Geology* **18**, 458–61.
- Chen HD, Zhang CG, Huang FX and Hou MC (2011) Filling process and evolutionary model of sedimentary sequence of Middle-Upper Yangtze craton in Hercynian-Indosinian (Devonian-Middle Triassic). *Acta Petrologica Sinica* **27**, 2281–98 (in Chinese with English abstract).
- Chen MQ (1989) A discussion of the origin of yangxin dolomite of lower Permian in southwest Sichuan. *Acta Sedimentologica Sinica* **7**, 45–50.
- Chen X, Zhao ZJ, Gao Y, Liu YH and Zhou H (2013) Middle Permian Maokou carbonate slope deposition and its significances for petroleum exploration in northern part of Sichuan Basin. *Marine Origin Petroleum Geology* **18**, 9–14 (in Chinese with English abstract).
- Combarrous MA and Bories SA (1975) Hydrothermal convection in saturated porous media. *Advances in Hydroscience* **10**, 231–307.
- Davies GR and Smith LB (2011) Structurally controlled hydrothermal dolomite reservoir facies: an overview: reply. *AAPG Bulletin* **90**, 1641–90.
- Deffeyes KS, Lucia FJ and Weyl PK (1965) Dolomitization of recent and Pliocene Pleistocene sediments by marine evaporite waters on Bonaire, Netherlands Antilles. In *Dolomitization and Limestone Diagenesis* (eds LC Pray and RC Murry), pp. 71–88. SEPM (Society for Sedimentary Geology), Tulsa, Special Publication.
- Deming D, Nunn JA and Evans DG (1990) Thermal effects of compaction-driven groundwater flow from overthrust belts. *Journal of Geophysical Research* **95**, 6669–83.
- Fabricius IL (2000) 10. Interpretation of burial history and rebound from loading experiments and occurrence of microstylolites in mixed sediments of Caribbean Sites 999 and 1001. In *Proceedings of the Ocean Drilling Program* (eds R Leckie, H Sigurdson, GD Acton and G Draper), pp. 177–90. College Station, Texas: Ocean Drilling Program, Scientific Results no. 165.
- Feng ZZ, Yang YQ, Jin ZK, He YB, Ww SH, Xin WJ, Bao ZD and Tan J (1996) Lithofacies paleogeography of the Permian of South China. *Acta Sedimentologica Sinica* **14**, 1–11 (in Chinese with English abstract).
- Friedman GM and Sanders JE (1967) Origin and occurrence of dolostones. *Developments in Sedimentology* **9**, 267–348.
- Fuchtbauer H (1974) *Sediments and Sedimentary Rocks*. New York: Halsted Press, pp. 303–5.
- Galy A, Yoffe O, Janney PE, Williams RW and Carignan J (2003) Magnesium isotope heterogeneity of the isotopic standard SRM980 and new reference materials for magnesium-isotope-ratio measurements. *Journal of Analytical Atomic Spectrometry* **18**, 1352–6.
- Garven G (2003) Continental-scale groundwater flow and geologic processes. *Annual Review of Earth & Planetary Sciences* **23**, 89–118.
- Geske A, Goldstein RH, Mavromatis V, Richter DK, Buhl D, Kluge T, John CM and Immenhauser A (2015) The magnesium isotope ($\delta^{26}Mg$) signature of dolomites. *Geochimica et Cosmochimica Acta* **149**, 131–51.
- Gillhaus A, Richter DK, Meijer J, Neuser RD and Stephan A (2001) Quantitative high resolution cathodoluminescence spectroscopy of diagenetic and hydrothermal dolomites. *Sedimentary Geology* **140**, 191–9.

- Goldstein RH and Reynolds TJ** (1994) *Systematics of Fluid Inclusions in Diagenetic Minerals*. Tulsa, OK: Society for Sedimentary Geology, Short Course no. 31, 199 p.
- Guo F, Fan W, Wang Y and Li C** (2004) When did the Emeishan mantle plume activity start? Geochronological and geochemical evidence from ultramafic-mafic dikes in Southwestern China. *International Geology Review* **46**, 226–34.
- Hao CY, Liu SW and Xu M** (2015) Current geothermal characteristics of Yangzi region in southern China. In *Proceedings of 2015 Annual Meeting of China Geoscience Union*. Beijing: Chinese Geophysical Society.
- He B, Xu YG, Huang XL, Luo ZY, Shi YR, Yang QJ and Yu SY** (2007) Age and duration of the Emeishan flood volcanism, SW China: Geochemistry and SHRIMP zircon U-Pb dating of silicic ignimbrites, post-volcanic Xuanwei Formation and clay tuff at the Chaotian section. *Earth & Planetary Science Letters* **255**, 306–23.
- He B, Xu YG, Wang YM, Luo ZY and Wang KM** (2005a) The magnitude of crustal uplift prior to the eruption of the emeishan basalt: inferred from sedimentary records. *Geotectonica et Metallogenia* **29**, 316–20 (in Chinese with English abstract).
- He B, Xu YG, Wang YM and Xiao L** (2005b) Nature of the Dongwu movement and its temporal and spatial evolution. *Earth Science* **30**, 89–96 (in Chinese with English abstract).
- He B, Xu YG, Xiao L, Wang KM and Shao ZL** (2003) Generation and spatial distribution of the Emeishan large igneous province: new evidence from stratigraphic records. *Acta Geologica Sinica* **77**, 194–202 (in Chinese with English abstract).
- He YB and Feng ZZ** (1996) Origin of fine-to-coarse grained dolostones of Lower Permian in Sichuan Basin and its peripheral region. *Journal of Jiangnan Petroleum Institute* **4**, 15–20.
- Hou MC, Wang WK, Zhang BJ, Wang W, Liu XH, Deng M, Pei SQ and Yang Y** (2013) Fluid types and activities of Emeishan basalt in Zhougong mountain-Hanwang field of Sichuan Province. *Acta Petrologica Sinica* **29**, 2709–18 (in Chinese with English abstract).
- Hsu KJ and Siegenthaler C** (1969) Preliminary experiments on hydrodynamic movement induced by evaporation and their bearing on the dolomite problem. *Sedimentology* **12**, 11–25.
- Hu WX, Zhu JQ, Wang XL, You XL and He K** (2014) Characteristics, origin and geological implications of the Cambrian microbial dolomite in Keping area, Tarim Basin. *Oil & Gas Geology* **35**, 860–69 (in Chinese with English abstract).
- Huang SJ** (1985) The degree of order and forming conditions of the dolomite of the third and fourth members of lower Triassic Jialingjiang formation in longmenxia, Quxian, Sichuan. *Journal of Mineralogy and Petrology* **5**, 57–62 (in Chinese with English abstract).
- Huang SJ** (1990) Cathodoluminescence and diagenetic alteration of marine carbonate minerals. *Sedimentary Facies and Palaeogeography* **4**, 9–15 (in Chinese with English abstract).
- Huang SJ** (1992) Relationship between cathodoluminescence and concentration of iron and manganese in carbonate minerals. *Mineralogy and Petrology* **4**, 74–79.
- Huang SJ** (1997) A study on carbon and strontium isotopes of late Paleozoic carbonate rocks in the Upper Yangtze Platform. *Acta Petrolei Sinica* **71**, 45–53 (in Chinese with English abstract).
- Huang SJ, Lan YF, Huang KK and Lv J** (2014) Vug fillings and records of hydrothermal activity in the Middle Permian Qixia Formation, western Sichuan Basin. *Acta Petrolei Sinica* **30**, 687–98 (in Chinese with English abstract).
- Huang SJ, Li XN, Huang KK, Lan YF, Lv J and Wang CM** (2012a) Authigenic noncarbonate minerals in hydrothermal dolomite of Middle Permian Qixia Formation in the west of Sichuan Basin, China. *Journal of Chengdu University of Technology (Science & Technology Edition)* **39**, 343–52 (in Chinese with English abstract).
- Huang SJ, Shi H, Zhang M, Shen LC, Liu J and Wu WH** (2001) Strontium isotope evolution and global sea-level changes of carboniferous and Permian Marine Carbonate, upper Yangtze platform. *Acta Sedimentologica Sinica* **19**, 481–87 (in Chinese with English abstract).
- Huang, SJ and Zhou SH** (2010) Carbon and strontium isotopes of Late Palaeozoic Marine Carbonates in the Upper Yangtze Platform, Southwest China. *Acta Geologica Sinica* **71**, 282–92.
- Huang Z, Chen T, Ren J and Bao H** (2012b) The characteristics of dolomite reservoir and trap accumulation in the middle assemblages of Ordovician in Ordos Basin, China. *Acta Petrolei Sinica* **33**, 118–24 (in Chinese with English abstract).
- Illing LV** (1959) *Cyclic carbonate sedimentation in the Mississippian at Moose Dome, southwest Alberta*. In *Proceedings of the Ninth Annual Field Conference*, Moose-Mountain Drumheller, pp. 37–52. Calgary, Alberta: CSPG Special Publications.
- James NP and Choquette PW** (1984) Diagenesis 9 limestones—the meteoric diagenetic environment. *Geoscience Canada* **11**, 161–94.
- Jiang QC, Hu S, Wang Z, Wang T, Li Q and Zhai X** (2014) Genesis of medium-macro-crystalline dolomite in Middle Permian in Sichuan Basin. *Oil & Gas Geology* **35**, 503–10 (in Chinese with English abstract).
- Jin ZK and Feng ZZ** (1999) Origin of dolostones of the Lower Permian in East Yunnan-West Sichuan dolomitization through leaching of basalts. *Acta Sedimentologica Sinica* **17**, 383–89 (in Chinese with English abstract).
- Kaufman J** (1994) Numerical models of fluid flow in carbonate platforms. *Journal of Sedimentary Research* **A64**, 128–39.
- Kenward PA, Goldstein RH, Brookfield AE, González LA and Roberts JA** (2012) Model for how microbial methane generation can preserve early porosity in dolomite and limestone reservoirs. *AAPG Bulletin* **96**, 399–413.
- Kohout FA, Henry HR and Banks JE** (1977) Hydrogeology related to geothermal conditions of the Floridan Plateau. In *The Geothermal Nature of the Floridan Plateau* (eds KL Smith and GM Griffin), pp. 1–34. Florida Department of Natural Resources Bureau, Geology Special Publications no. 21.
- Korte C, Jasper T, Kozur HW and Veizer J** (2006) ⁸⁷Sr/⁸⁶Sr record of Permian seawater. *Palaeogeography, Palaeoclimatology, Palaeoecology* **240**, 89–107.
- Land LS** (1972) Contemporaneous dolomitization of middle Pleistocene reefs by meteoric water, North Jamaica. *AAPG Bulletin* **56**, 635.
- Li B, Gu XC, Wen SM, Han RS, Sheng R, Xx GD, Cao Y, Wu H and Zou GF** (2012) Effect of Emeishan basalt in northeast Yunnan on lead and zinc mineralization. *Mineral Resources and Geology* **26**, 95–100 (in Chinese with English abstract).
- Li GH, Li X, Song SJ, Song WH and Yang XN** (2005) Dividing Permian into 3 series and its significance in Sichuan Basin. *Natural Gas Exploration & Development* **28**, 20–25 (in Chinese with English abstract).
- Li HM, Mao JW and Zhang CQ** (2011) Geochemistry of fluid inclusions of the basalt copper deposits in adjacent area of Northeastern Yunnan and Western Guizhou, China. *Journal of Earth Sciences and Environment* **33**, 14–23 (in Chinese with English abstract).
- Li W, Beard BL, Li C, Xu H and Johnson CM** (2015) Experimental calibration of Mg isotope fractionation between dolomite and aqueous solution and its geological implications. *Geochimica et Cosmochimica Acta* **157**, 164–81.
- Lind IL** (1993) Stylolites in chalk from Leg 130, Ontong Java Plateau. In *Proceedings of the Ocean Drilling Program* (eds WH Berger, JW Kroenke and LA Mayer), pp. 445–51. College Station, Texas: Ocean Drilling Program, Scientific Results no. 130.
- Liu CY and Zhu RX** (2009) Discussion on geodynamic significance of the Emeishan basalts. *Earth Science Frontiers* **16**, 52–69 (in Chinese with English abstract).
- Longman MW** (1980) Carbonate diagenetic texture from nearsurface diagenetic environments. *AAPG* **64**, 461–87.
- Lu W, Cui BQ, Yang SQ and Zhang P** (1992) Strontium isotopic evolution of the Permian marine carbonates and implications. *Journal of Mineralogy and Petrology* **12**, 80–7 (in Chinese with English abstract).
- Luo ZL, Jin YZ, Zhu XY and Zhao XK** (1988) On Emei taphrogenesis of the upper Yangtze platform. *Geological Review* **34**, 15–28.
- Luo ZL, Sun W, Han JH and Wang RJ** (2012) Effect of Emei mantle plume on the conditions of Permian accumulation in middle-upper Yangtze Area. *Earth Science Frontiers* **19**, 144–54 (in Chinese with English abstract).
- Machel HG** (1985) Cathodoluminescence in calcite and dolomite and its chemical interpretation. *Geoscience Canada* **12**, 139–47.
- Machel HG** (2004) Concepts and models of dolomitization: a critical reappraisal. In *The Geometry and Petrogenesis of Dolomite Hydrocarbon Reservoirs* (eds CJR Braithwaite, G Rizzi and G Darke), pp. 7–63. Geological Society of London, Special Publication no. 235.
- Machel HG and Anderson JH** (1989) Pervasive subsurface dolomitization of the Nisku Formation in central Alberta. *Journal of Sedimentary Petrology* **59**, 891–911.

- Machel HG, Cavell PA, Buschkuhle BE and Michael K** (2000) Tectonically induced fluid flow in Devonian carbonate aquifers of the Western Canada Sedimentary Basin. *Journal of Geochemical Exploration* **69–70**, 213–17.
- Mao DM** (1991) Trace element geochemistry of the Emeishan Basalt in Western Guizhou. *Journal of Guizhou Institute of Technology* **20**, 82–91 (in Chinese with English abstract).
- Mazzullo SJ** (2000) Organogenic dolomitization in peritidal to deep-sea sediments. *Journal of Sedimentary Research* **70**, 10–23.
- McArthur JM, Howarth RJ and Bailey TR** (2001) Strontium isotope stratigraphy: LOWESS Version 3: best fit to the marine Sr-isotope curve for 0–509 Ma and accompanying look-up table for deriving numerical age. *Journal of Geology* **109**, 155–70.
- Meade F** (2010) Igneous rocks and processes: a practical guide – by Robin Gill. *Geographical Journal* **176**, 375–376.
- Ministry of Geology and Mineral Resources of PR China** (1982) *Regional Geology of Yunnan*. Beijing: Geology Press, pp. 160–78.
- Morlot A and Haidinger W** (1847) Ueber Dolomit und seine künstliche Darstellung aus Kalkstein. In *Naturwissenschaftliche Abhandlungen* (ed. W Haidinger), pp. 305–15. Vienna: Hofbuchhandlung Wilhelm Braumüller.
- Mountjoy EW and Halim-Dihardja MK** (1991) Multiple phase fracture and fault-controlled burial dolomitization, Upper Devonian Wabamun Group, Alberta. *Journal of Sedimentary Petrology* **61**, 590–12.
- Oliver J** (1986) Fluids expelled tectonically from orogenic belts: their role in hydrocarbon migration and other geologic phenomena. *Geology* **14**, 99–102.
- Phillips OM** (1991) *Flow and Reactions in Permeable Rocks*. Cambridge: Cambridge University Press.
- Raffensperger JP and Vlassopoulos D** (1999) The potential for free and mixed convection in sedimentary basins. *Hydrogeology Journal* **7**, 505–20.
- Rosenbaum J and Sheppard SMF** (1986) An isotopic study of siderites, dolomites and ankerites at high temperatures. *Geochimica et Cosmochimica Acta* **50**, 1147–50.
- Sanford WE, Whitaker FF, Smart PL and Jones G** (1998) Numerical analysis of seawater circulation in carbonate platforms; I, Geothermal convection. *American Journal of Science* **298**, 801–28.
- Sharp Z** (2007) *Principles of Stable Isotope Geochemistry*. Upper Saddle River, New Jersey: Pearson Education.
- Shukla V, Gregg JM and Sibley DF** (1984) Epigenetic dolomitization and the origin of xenotopic dolomite texture; discussion and reply. *Journal of Sedimentary Research* **54**, 908–21.
- Simms M** (1984) Dolomitization by groundwater-flow system in carbonate platforms. *AAPG Bulletin* **34**, 411–20.
- Song WH** (1985) Distribution of Permian dolomite and natural gas exploration in the Sichuan Basin. *Natural Gas Industry* **6**, 32–33 (in Chinese with English abstract).
- Su W, Jiang QC, Chen ZY, Wang ZC, Jiang H, Bian CS, Feng QF and Wu YL** (2015) Sequence stratigraphic features of Middle Permian Maokou Formation in the Sichuan Basin and their controls on source rocks and reservoirs. *Natural Gas Industry* **35**, 34–43 (in Chinese with English abstract).
- Sun S** (1995) Dolomite reservoirs: porosity evolution and reservoir characteristics. *AAPG Bulletin* **79**, 186–204.
- Tian JC, Lin XB, Zhang X, Peng SF, Yang CY, Luo S and Xu L** (2014) The genetic mechanism of shoal facies dolomite and its additive effect of Permian Qixia Formation in Sichuan Basin. *Acta Petrologica Sinica* **30**, 679–86 (in Chinese with English abstract).
- Tóth J** (1988) Ground water and hydrocarbon migration. In *Hydrogeology* (eds W Back, JS Rosenhein and PR Saeber), pp. 485–502. Boulder, CO: Geological Society of America, The Geology of North America.
- Vasconcelos C and McKenzie JA** (1997) Microbial mediation of modern dolomite precipitation and diagenesis under anoxic conditions (Lagoa Vermelha, Rio de Janeiro, Brazil). *Journal of Sedimentary Research* **67**, 378–90.
- Vasconcelos C, McKenzie JA, Warthmann R and Bernasconi SM** (2005) Calibration of the $\delta^{18}\text{O}$ paleothermometer for dolomite precipitated in microbial cultures and natural environments. *Geology* **33**, 317–20.
- Veizer J, Ala D, Azmy K, Bruckschen P, Buhl D, Bruhn F, Gorden GAF, Diener A, Ebner S, Godderis Y, Jasper T, Korte C, Pawellek F, Podlaha OG and Strauss H** (1999) $^{87}\text{Sr}/^{86}\text{Sr}$, $\delta^{13}\text{C}$ and $\delta^{18}\text{O}$ evolution of Phanerozoic seawater. *Chemical Geology* **161**, 59–88.
- Wang H, Shen H, Huang D, Shi X, Li Y, Yuan X and Yang Y** (2014) Origin and distribution of hydrothermal dolomites of the Middle Permian in the Sichuan Basin. *Natural Gas Industry* **34**, 25–32 (in Chinese with English abstract).
- Wang J, Huang SY, Huang GS and Wang JY** (1986) Basic characteristics of the Earth's temperature distribution in southern China. *Acta Geologica Sinica* **60**, 91–106.
- Wang ML, Zhou JG, Chen DX, Hao Y, Peng HJ, Wang C, Jiang YT and Xie MX** (2013) Research advances of dolomite genesis models and discussion on applicable models. *Marine Origin Petroleum Geology* **18**, 31–40 (in Chinese with English abstract).
- Wang X, Gao G, Li JY, Ge DW and Zhang WW** (2017) Hydrocarbon expulsion of stylonite and matrix in carbonate rocks: a case study from the Ordovician and Carboniferous carbonate rocks in Eastern Sichuan Basin. *Oil & Gas Geology* **38**, 534–42.
- Wang Y and Jin Y** (1997) The formation of dolomite and paleokarst of the lower Permian series in Sichuan Basin and the relation to the Emei taphrogenesis. *Journal of Chengdu University of Technology (Science & Technology Edition)* **24**, 8–16 (in Chinese with English abstract).
- Warthmann R, Van lith Y, Vasconcelos C, McKenzie JA and Karpoff AM** (2000) Bacterially induced dolomite precipitation in anoxic culture experiments. *Geology* **28**, 1091–94.
- Whitaker FF, Jones G and Smart P** (2003) From conceptual to numerical models of dolomitization. In *Proceedings of the 12th Bathurst Meeting, International Conference of Carbonate Sedimentologists*, 8–10 July 2003, Durham.
- Whitaker FF, Smart PL and Jones G** (2004) Dolomitization: from conceptual to numerical models. In *The Geometry and Petrogenesis of Dolomite Hydrocarbon Reservoirs* (eds CJR Braithwaite, G Rizzi and G Darke), pp. 99–139. Geological Society, London, Special Publication no. 235.
- Whitaker FF, Wilson AM, Sanford WE and Smart PL** (2002) Spatial patterns and rates of dolomitization and anhydritization during geothermal convection in carbonate platforms. In *The Geometry and Petrogenesis of Dolomite Hydrocarbon Reservoirs* (convenors G Rizzi, G Darke and CJR Braithwaite). Final Programme and Abstracts. Geological Society of London, Petroleum Group.
- Wilson AM, Sanford WE, Whitaker FF and Smart PL** (2001) Spatial patterns of diagenesis during geothermal circulation in carbonate platforms. *American Journal of Science* **301**, 727–52.
- Wilson EN, Hardie LA and Phillips OM** (1990) Dolomitization front geometry, fluid flow patterns, and the origin of massive dolomite: the Triassic Latemar buildup, Northern Italy. *American Journal of Science* **290**, 741–96.
- Wo YJ, Zhou Y and Xiao KH** (2007) The burial history and models for hydrocarbon generation and evolution in the marine strata in southern China. *Sedimentary Geology and Tethyan Geology* **27**, 94–100 (in Chinese with English abstract).
- Wood JR and Hewett TA** (1982) Fluid convection and mass transfer in porous sandstones: a theoretical approach. *Geochimica et Cosmochimica Acta* **46**, 1707–13.
- Wright DT and Wacey D** (2004) Sedimentary dolomite: a reality check. In *The Geometry and Petrogenesis of Dolomite Hydrocarbon Reservoirs* (eds CJR Braithwaite, G Rizzi and G Darke), pp. 65–74. Geological Society, London, Special Publication no. 235.
- Yuan YS, Ma YS, Hu SB, Guo TL and Fu XY** (2006) Present-day geothermal characteristics in South China. *Chinese Journal of Geophysics* **49**, 1118–26 (in Chinese with English abstract).
- Zeng L and Wan MX** (2004) Dolomite sequentiality and its application to petroleum geology. *Natural Gas Exploration and Development* **27**, 64–6 (in Chinese with English abstract).
- Zenger DH and Dunham JB** (1980) Concepts and models of dolomitization: an introduction. In *Concepts and Models of Dolomitization* (eds DH Zenger, JB Dunham and RL Ethington), pp 285–6. Society of Economic Paleontologists and Mineralogists, Tulsa, Special Publication no. 17.
- Zenger DH and Hardie LA** (1987) Dolomitization; a critical view of some current views; discussion and reply. *Journal of Sedimentary Research* **57**, 166–83.
- Zhang J, Shou JF, Zhang TF, Pan LY and Zhou JG** (2014) New approach on the study of dolomite origin: the crystal structure analysis of dolomite. *Acta Sedimentologica Sinica* **32**, 550–9 (in Chinese with English abstract).

- Zhang XF, Hu WX and Zhang JT** (2006) Critical problems for dolomite formation and dolomitization models. *Geological Science and Technology Information* **25**, 32–40 (in Chinese with English abstract).
- Zhang Y** (1982) Dolomitization in Permian rocks in Sichuan Basin. *Acta Petroli Sinica* **3**, 33–37, 105–106 (in Chinese with English abstract).
- Zheng H, Wu M, Wu X, Zhang T and Liu C** (2007) Oil-gas exploration prospect of dolomite reservoir in the Lower Paleozoic of Tarim Basin. *Acta Petroli Sinica* **28**, 1–8 (in Chinese with English abstract).
- Zheng RC, Shi JN, Luo AJ, Li S and Li G** (2008) Comparative study on geochemical behaviors of dolomite reservoirs in Northeast Sichuan Basin. *Natural Gas Industry* **28**, 16–21 (in Chinese with English abstract).
- Zhou Y, Chen HD, Wang CS, Jin ZJ, Tang LJ, Wang ZY and Liang XW** (2005) The Middle Permian sequence stratigraphy of the Mid-Yangtze area. *Journal of Stratigraphy* **29**, 270–80 (in Chinese with English abstract).